Dear Marit-Solveig Seidenkrantz and reviewers,

We thank you for giving us the opportunity to revise our manuscript. We also appreciate the reviewer's constructive comments and suggestions that helped to improve the manuscript. In the revised version we marked changes in red. In the reply letter below we explain how we addressed every point raised by you and the reviewers.

Looking forward to hearing from you.

Thank you and best regards.
Mingming Ma on behalf of all co-authors

Editor

Before potential publication, the authors should add a discussion on the mechanisms causing the described climate change. However, at present the review process can start and an expansion of the discussion can wait till after the first round of reviews, if these are sufficiently favourable.

Response: We added a short discussion on the potential mechanisms that probably related to the paleomonsoon in Lines 513-530 as you suggested.

Referee 1

Detailed comparison of paleoclimatic records between land and ocean is essential to evaluate the global paleoclimate pattern. This study constructed new data across theCretaceous-Palaeogene boundary boundary in the Nanxiong Basin (SE China). On the basis of previous paleomagnetic studies, authors provided a new interpretation of magnetostratigraphy, and found that patterns of paleoclimatic proxies (magnetic susceptibility and Neel temperature) from the studied profile are similar to the global d18O curves. Then they divided the results into three stages with distinct patterns. Overall, this study is interesting because it provides new results from the terrestrial media and thus has global paleoclimatic significances. However, the following two issues need further clarifications:

1) The fidelity of the magnetostratigraphy Authors provided an new interpretation in section 4.1. This new interpretation is the foundation of the whole story. From lines 302-309, there are still presence of ambiguities even for the new interpretation. Therefore, more subtle discussions on the magnetostratigraphy are still needed.

Response: We added more subtle discussions on the magnetostratigraphy, please see lines 336-347.

2) Magnetic susceptibility is a complicated proxy. Authors need more discussions on the exact variation mechanism for susceptibility. It seems that hematite is the dominant magnetic minerals, it will be more direct to measure hematite-related proxies, e.g., HIRM, DRS results, etc.

Response: 1) We added more discussions on the variation mechanism for susceptibility that probably related to the paleomonsoon, please see lines 513-530.

2) HIRM has been shown in section 3.3 and Fig. 4 already.

3) We added DRS results in the revised manuscript, please see lines 175-180, 184-196 and Fig. 2.

Referee 2

In this paper, Ma et al. proposed a new age model for this section and reviewed the paleoenvironment and paleoclimate changes during the K-Pg boundary interval. Overall, I commend the authors for applying new method on this topic and propose new ideas. However, the interpretations and conclusions need to be major modified before publication.

1. The authors claimed that the C30R and C31N was missing due to the covered strata. However, this is just the authors' speculation, and there is no further evidences. The authors also concluded that the age between the Zhenshui and Zhutian formations is ~71.5 Ma according to their new age model. However, this age is inconsistent with the biostratigraphic data they cited, which suggests the Zhutian Formation is lower

Santonian-Campanian in age.

Response: We added more subtle discussions on the magnetostratigraphy, please see lines 336-347.

2. The authors suggested that "the haematite was the dominant magnetic mineral in the red strata, and the variation trend of magnetic susceptibility was consistent with the oxygen isotope records from deep-sea sediments, which indicates that the pedogenic intensity was controlled by global climate". I can not understand the logic relationship in this sentence. Are their samples for magnetic susceptibility all collect from the palaeosls? Please clarify. In addition, if the age model is not valid, the consistency between the magnetic susceptibility and d18O would not exist.

Response: 1) Yes, we suggested that all the samples were collected from palaeosols, the difference is that moderately to fully mature soils with diagnostic characters such as Bk horizons, wormholes and root traces formed in sandy mudstone and muddy sandstone layers. No typical palaeosols were found in the coarse sandstone or conglomerate layers because of the lack of essential conditions for soil formation, but many root traces were preserved which can be called "weakly developed soils". Please see more details in section 4.2. Haematite was generated during pedogenic processes, the relationship between χ and haematite content can be explained by the "pedogenic-plus hypothesis": more haematite formed during warmer and wetter periods with stronger pedogenesis, and caused a higher χ, and opposite conditions yielded lower χ values. So we concluded that the pedogenic intensity indicated by the content of haematite (i.e. χ) was controlled by global climate. However, we would like to change this sentence to "the haematite was the dominant magnetic mineral in the red strata, and the variation trend of magnetic susceptibility was consistent with the oxygen isotope records from deep-sea sediments, which indicates that the content of haematite was controlled by global climate" (lines 33-36), so as not to confuse the readers.

2) As age model, please see last response.

3. The authors classified the climate evolution into three stages. But the proposed trend is similar to that established by other proxies and no substantial promotion, still qualitative.

Response: We agree with your comments that the constructed climate evolution revealed by magnetic parameters is still qualitative, however, it shows more details than other proxies or the marine record, such as the several sub-fluctuations during each stage, which probably indicates that the climate changes from 72 to 62.8 Ma were extremely instable with more fluctuations, and this needs our further work to provide quantitative and higher resolution results in the future. See lines 596-601.

However, we add more discussions on the potential mechanisms causing the described climate change that is not mentioned in previous studies, please see lines 513-530.

Palaeoclimate evolution across the Cretaceous–Palaeogene boundary in the Nanxiong Basin (SE China) recorded by red strata and its correlation with marine records

Mingming Ma[a,b], Xiuming Liu[a,b,c*], Wenyan Wang[a,b]

[a]*Institute of Geography, Fujian Normal University, Fuzhou, 350007, China; E-mail: xliu@fjnu.edu.cn*

[b]*Key Laboratory for Subtropical Mountain Ecology (Funded by the Ministry of Science and Technology and Fujian Province), College of Geographical Sciences, Fujian Normal University, Fuzhou, 350007, China;*

[c]*Department of Environment and Geography, Macquarie University, NSW 2109, Australia.*

Abstract: The climate during the Cretaceous Period represented one of the "greenhouse states" of Earth's history. Significant transformation of climate patterns and a mass extinction event characterised by the disappearance of dinosaurs occurred across Cretaceous–Palaeogene boundary. However, most records of this interval are derived from marine sediments. The continuous and well-exposed red strata of the Nanxiong Basin (SE China) provide ideal material to develop continental records. Considerable research into stratigraphic, palaeontological, chronologic, palaeoclimatic, and tectonic aspects has been carried out for the Datang Profile, which is a type section of a non-marine Cretaceous–Palaeogene stratigraphic division in China. For this study, we reviewed previous work and found that: 1) the existing chronological framework of the Datang Profile is flawed; 2) precise palaeoclimatic reconstruction is lacking because of the limitations of sampling resolution (e.g. carbonate samples) and/or the lack of efficient proxies; and 3) comparisons of climate

changes between marine and continental records are lacking. To resolve these problems, detailed field observations and sampling, as well as environmental magnetic and rare earth element (REE) measurements, were carried out. The results show that: 1) more accurate ages of the Datang Profile range from 72 Ma to 62.8 Ma, based on a combination of the most recently published radiometric, palaeontological and palaeomagnetic ages; 2) there is considerable evidence of palaeosol generation, which indicates that the red strata formed in a long-term hot, oxidizing environment that lacked of underwater condition; 3) haematite was the dominant magnetic mineral in the red strata, and the variation trend of magnetic susceptibility was consistent with the oxygen isotope records from deep-sea sediments, which indicates that the content of hematite was controlled by global climate; and 4) the palaeoclimate changes from 72 Ma to 62.8 Ma in the Nanxiong Basin were consistent with global patterns, and can be divided into three stages: a relatively hot and wet stage during 72–71.5 Ma, a cool and arid stage during 71.5–66 Ma, and a relatively hot and wet stage again during 66–62.8 Ma with a notable drying and cooling event at 64.7–63.4 Ma. Moreover, there are several sub-fluctuations during each stage. This work provides basic information for further palaeoclimate reconstruction with higher resolution and longer time scales for the Cretaceous to Palaeocene in the Nanxiong Basin, and may even help to test ocean–land climate interactions in the future.

Keywords: Cretaceous–Palaeogene boundary; Nanxiong Basin; Palaeosol; Environmental magnetism; Palaeoclimate evolution

1 Introduction

The Earth existed in a greenhouse state during the Late Cretaceous (Hay, 2011; Friedrich et al., 2012; Wang et al., 2014); palaeoclimate studies show that based on

50 marine records, the seawater surface temperature near the equator reached up to 36℃

51 during the Late Cretaceous (Linnert et al., 2014), and reconstructed CO_2

52 concentrations reach up to 837 ppm across the Cretaceous–Tertiary boundary, as

53 recorded in palaeosol carbonates in NE China (Huang et al., 2013). The correlation

54 between extreme greenhouse climate and high CO_2 concentration across this

55 boundary may provide insights for global warming in the present (Wang et al., 2013b).

56 The palaeotemperature decreased significantly from the Mesozoic Era to the Cenozoic

57 (Zachos et al., 2001; Hay, 2011), and a mass extinction event occurred across the

58 Cretaceous–Palaeogene boundary (Schulte et al., 2010; Renne et al., 2013); climate

59 changes and biological evolution during this interval have therefore become a

60 research hotspot. However, most studies of climate change across the Cretaceous–

61 Palaeogene boundary have been derived from marine records (Huber et al., 1995;

62 Barrera and Savin, 1999; Cramer et al., 2009; Friedrich et al., 2012; Bodin et al.,

63 2015). Terrestrial palaeoclimate records are few, and published comparisons and

64 correlations between marine and terrestrial palaeoclimate records are even fewer

65 (Wang et al., 2013b).

66   There are many basins with Cretaceous continental sediments distributed across

67 China (Li et al., 2013), such as the Songliao Basin (NE China, Wu et al., 2009;

68 Bechtel et al., 2012; Chamberlain et al., 2013; Wang et al., 2013a, b; Wan et al.,

69 2013), the Sichuan Basin (SW China; Li, 1988; Huang et al., 2012; Li et al., 2015),

70 and the Nanxiong Basin (SE China; Zhao et al., 1991, 2002, 2009; Buck et al., 2004;

71 Clyde et al., 2010; Li et al., 2010; Wang et al., 2015), which provide ideal records for

72 investigation of Cretaceous climate change. Among these basins, continuous and

73 well-exposed red strata consisting of mudstone and sandstone are preserved in the

74 Nanxiong Basin, and many fossils have been found in these red strata, such as

75 charophytes, palynomorphs, ostracods, dinosaurs, dinosaur eggs, and mammals

76 (Zhang, 1992; Zhang et al., 2006, 2013; Clyde et al., 2010; Li et al., 2010). Many

77 studies have focused on the Datang Profile, which is also called the CGY–CGD

78 profile by Chinese and Germany scientists (Zhao et al., 1991; Yang et al., 1993; Zhao

79 & Yan, 2000). Studies of this profile have investigated its stratigraphy, palaeontology,

80 geochronology, and palaeoclimatology (Zhao et al., 1991; Zhang, 1992; Zhang et al.,

81 2006, 2013; Clyde et al., 2010; Tong et al., 2013; Wang et al., 2015), because it spans

82 from the Upper Cretaceous to the Lower Palaeocene and is a type section for non-

83 marine Cretaceous–Palaeogene stratigraphic division in China. However, precise

84 reconstruction of the palaeoclimatic evolution of this section and comparison with

85 marine records are still lacking because of the lack of efficient proxies. Moreover,

86 many Cretaceous–Palaeogene records are also lacking from low-latitudes in this part

87 of the word, therefore, it is of great significance to carry out paleoclimate change

88 studies here.

89   Environmental magnetism as a proxy has been widely used in the studies of

90 palaeoclimatic changes in Quaternary loess–palaeosol successions (Evans & Heller,

91 2001; Hao & Guo, 2005; Maher & Possolo, 2013; Maher, 2016), Tertiary red clay

92 successions (Liu et al., 2003; Nie et al., 2008; Zhao et al., 2016), and other older

93 aeolian deposits (Hao et al., 2008; Tao et al., 2011), as well as in studies of lake

94 sediments (Snowball et al., 1999; Fu et al., 2015; Hu et al., 2015), and marine

95 sediments (Larrasoaña et al., 2008; Peters et al., 2010). In this paper, we review

96 previous work (mainly in terms of geochronology and palaeoclimatology) and report

97 some defects in the established chronological framework and palaeoclimatic record.

98 Therefore, the aims of this work are to: 1) establish a new chronological framework

99 for the Datang Profile, 2) reinterpret the environment in which the red strata formed, 3)

100   try to reconstruct the palaeoclimatic changes using magnetic parameters, and 4)

101   compare the terrestrial records with marine records to provide reliable terrestrial

102   records for future investigation of ocean–land climate interactions.

103   **2   Geological background, materials, and methods**

104   **2.1 Geological background**

105   The Nanxiong Basin (25°03′–25°16′N, 114°08′–114°40′E) is a rift basin that

106   developed on pre-Jurassic basement, and is controlled by the Nanxiong Fault (Shu et

107   al., 2004). Most of this basin is located in northern Guangdong Province, SE China

108   (Fig. 1A). The basin is elongated with its axis oriented northeast–southwest (Fig. 1B),

109   and is distributed in an area between the Zhuguang and Qingzhang granites (Shu et al.,

110   2004). The modern mean annual rainfall and temperature are ~1,555 mm and ~19.9℃,

111   respectively (data from China Meteorological Data Service Center). Continuous

112   successions of red fluvial–lacustrine clastics, with a maximum thickness of more than

113   7 km, are preserved in the basin. These successions span the Upper Cretaceous,

114   represented by the dinosaur-bearing Nanxiong Group (Changba, Jiangtou, Yuanpu,

115   Dafeng, Zhutian, and Zhenshui Formations), and the Lower Palaeocene, represented

116   by the mammal-bearing Luofuzhai Group (Shanghu, Nongshan, and Guchengcun

117   Formations) (Zhang et al., 2013). Components of conglomerate and coarse-grained

118   sandstone in the basin are similar to those of adjacent strata; moreover, pebbles found

119   in the basin are relatively coarse, poorly sorted, and sharp-edged, which implies that

120   the sediment source was not far from the basin (Shu et al., 2004), and that erosion was

121   stable though the Late Cretaceous to Early Palaeocene (Yan et al., 2007).

122
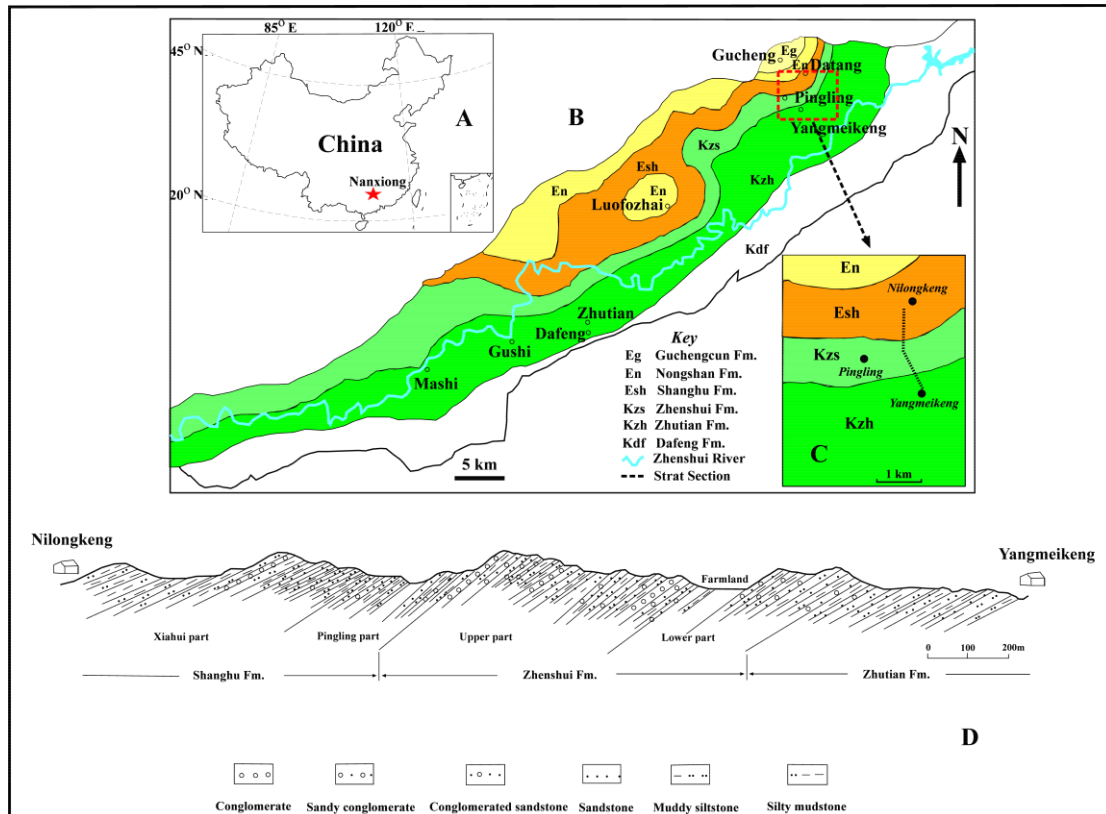
Fig. 1 Sketch map of the Nanxiong Basin: A) location of Nanxiong Basin, B)

stratigraphy of the Nanxiong Basin (from the Dafeng Formation to the Guchengcun

Formation, modified from Li et al., 2010), C) sampling route of the Datang Profile, D)

stratigraphy of the Datang Profile (modified from Zhang et al., 2006). Note that the

Zhutian Formation in Datang Profile is just the top part of the whole Zhutian

Formation.

Several profiles in the basin have been investigated since the 20th century (Zhao

et al., 1991, 2002; Zhang & Li, 2000; Zhang et al., 2006, 2013; Zhang & Li, 2015). Of

these profiles, the Datang Profile (Fig. 1C), with a vertical thickness of ~700 m, was

the most thoroughly investigated because of clear stratigraphic succession and

abundant fossils. The Datang Profile consists of three formations (Fig. 1D, Zhang et

al., 2006); from bottom to top these are the Zhutian Formation (105 m), the Zhenshui

135   Formation (295.5 m), and the Shanghu Formation (288.3 m), which are described in

136   detail below (Zhang et al., 2006; Wang, 2012; Zhang, 2016).

137   The Zhutian Formation consists mainly of brown-red, dark purple muddy

138   siltstone, and silty mudstone with fine sandstone interbeds. Large quantities of

139   ostracods and charophytes, and minor amounts of gastropods, conchostracans, and

140   dinosaur footprints have been discovered. Several moderately to fully mature

141   palaeosol layers with calcareous nodules generated in this formation.

142   The Zhenshui Formation is predominantly composed of coarse clastic deposits,

143   represented by grey-purple sandstone and conglomerate with red silty mudstone

144   interbeds. This formation is rich in vertebrate and dinosaur eggs, with minor amounts

145   of ostracods, charophytes, bivalves, and gastropods. A few moderately to fully mature

146   palaeosol layers generated in this formation.

147   The Shanghu Formation is predominantly composed of purple and dark brown

148   muddy siltstone and silty mudstone with numerous calcareous nodules and thin

149   interbeds of sandstone and conglomerate. This formation is rich in microfossils such

150   as ostracods and charophytes, and also contains fossils of mammals, turtles,

151   gastropods, and pollen. A great deal of moderately to fully mature palaeosol layers

152   generated in this formation.

153   **2.2 Materials and methods**

154   Powder samples were collected from the Datang Profile; because of strong

155   weathering of the Zhenshui Formation, the sampling intervals for this formation were

156   larger than those for the other formations. To eliminate the effects of particle size on

157   magnetic parameters, the selected samples were mainly muddy siltstone or silty

mudstone. All samples were dried naturally in a laboratory, gently ground to disaggregate the grains, and then packed into small non-magnetic plastic boxes (8 cm^3) before measurement. Magnetic susceptibility (χ) was measured using a Bartington MS2-B meter at 470 Hz and then normalised by mass. Anhysteretic remanent magnetisation (ARM) was imparted with a peak AF field of 100 mT and a DC bias field of 0.05 mT using a Molspin alternating field demagnetiser, and then measured with a Molspin Minispin magnetometer. Isothermal remanent magnetisation (IRM) was conducted using a Molspin 1 T pulse magnetiser and measured by employing the Minispin magnetometer. The IRM at 1 T was regarded as saturation IRM (SIRM). Backfield remagnetisation of SIRM was carried out using reverse fields at 10 mT steps, and remanence coercivity (Bcr) was calculated using linear interpolation. High-temperature magnetic susceptibility curves (κ-T curves) were obtained using an Agico KLY-3 Kappabridge with a CS-3 high-temperature furnace.

Rare earth element (REE) measurements were completed using an X-SERIES inductively coupled plasma-mass spectrometer (ICP-MS). Before measurement, bulk samples were successively treated with HF and HNO_3 (3:1), $HClO_4$, HNO_3 (HNO_3:H_2O = 1:2), and ultrapure water.

The diffuse reflectance spectroscopy (DRS) of fine powdered samples (<38 μm, both before and after heated by 200℃ for 2 hours) was recorded from 190 to 1100 nm in 5 nm steps, using a UV-2600 spectrophotometer (Shimadzu Instruments Manufacturing Co., Ltd.). In this study, only the records from 400 to 700nm (visible spectrum) were shown and the first derivative spectral patterns were calculated to determine the presence of hematite/goethite.

All measurements were conducted at the Key Laboratory for Subtropical Mountain Ecology, Fujian Normal University.

3 Results

3.1 DRS

The DRS technique provides a quantitative method to determine the haematite and goethite, which has been successfully used in marine deposits (Balsamand Deaton, 1991) and loess sections from the Chinese Loess Plateau (Ji et al., 2001; Balsam et al., 2004; Torrent et al., 2007). The peaks of the bands at 575 nm and 435/535 nm in the first derivative spectral (FDV) patterns are interpreted as haematite and goethite, respectively. However, the clay minerals (such as Chlorite and Illite) also show peaks at 435nm (Ji et al., 2006). In Fig.2, all curves show significant peak at ~575 nm, indicating the existence of haematite. Besides, there are small peaks at ~440nm which maybe related to goethite or clay minerals. However, the ~440nm peaks are still exist even after 200℃heated for 2 hours (Fig. 2B). Goethite will be transformed to haematite under 200℃ (Ma et al., 2013), so the ~440nm peaks probably related to the clay minerals but not goethite.
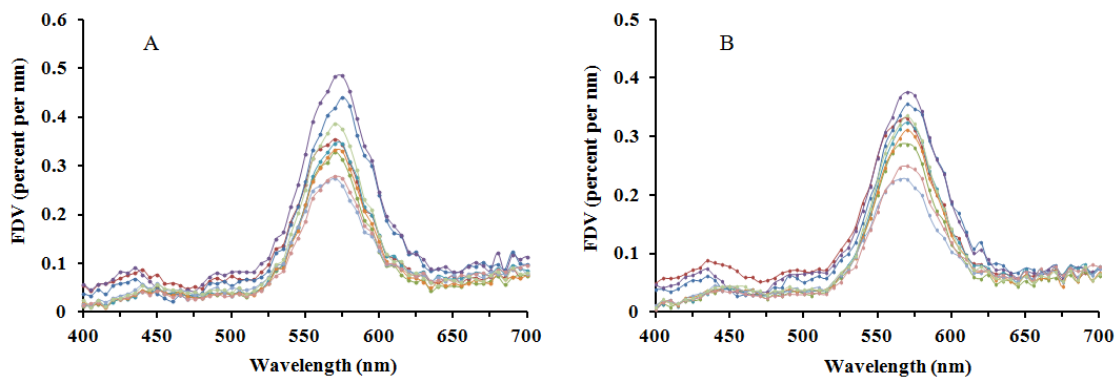
Fig.2 First-derivative curves of pilot samples before (A) and after 200℃ heated (B). After 200℃ heated, the presence of first-derivative peaks are similar with before heated. All curves show significant peak at ~575 nm, indicating the existence of haematite.

3.2 κ-T curves

High-temperature κ-T curves can be used to identify magnetic phases according to their Curie/Neel temperatures (Tc/T_N) or specific decomposition temperatures during the heating process; for example, the Tc/T_N of magnetite and haematite are ~580℃ (Smith, 1956; Levy et al., 2012) and ~670℃ (Lu & Meng, 2010), respectively. Partial substitution of Fe in magnetite or haematite with Ti or Al will decrease their Tc temperatures (Jiang et al., 2012, 2015). Maghemite generated during pedogenic processes is generally unstable during heating, as represented by its transformation to haematite at 300–400℃ (Liu et al., 1999). In addition to being affected by the magnetic mineral type, κ-T curves are also affected by magnetic particle size due to that some fine particles could change their domain state during the heating/colling process (Liu et al., 2005).

The κ-T curves of pilot samples from the Datang Profile are similar (Fig. 3); heating curves decrease with increasing temperature from room temperature to ~200℃, which suggests the presence of paramagnetic minerals (Evans & Heller, 2003). And then gradually increases from 200℃ to ~500-600℃, which may be related to the unblocking effects of fine magnetic particles (Liu et al., 2005). After this step, a T_N of about 640–660℃ is shown, which indicates the presence of haematite, and the decreased T_N temperatures may be related to partial substitution of Fe elements with Al (Jiang et al., 2013, 2014). Most heating and cooling curves are nearly reversible, which indicates that no new magnetic minerals are generated during the heating process; therefore, the haematite is original in the samples.

224
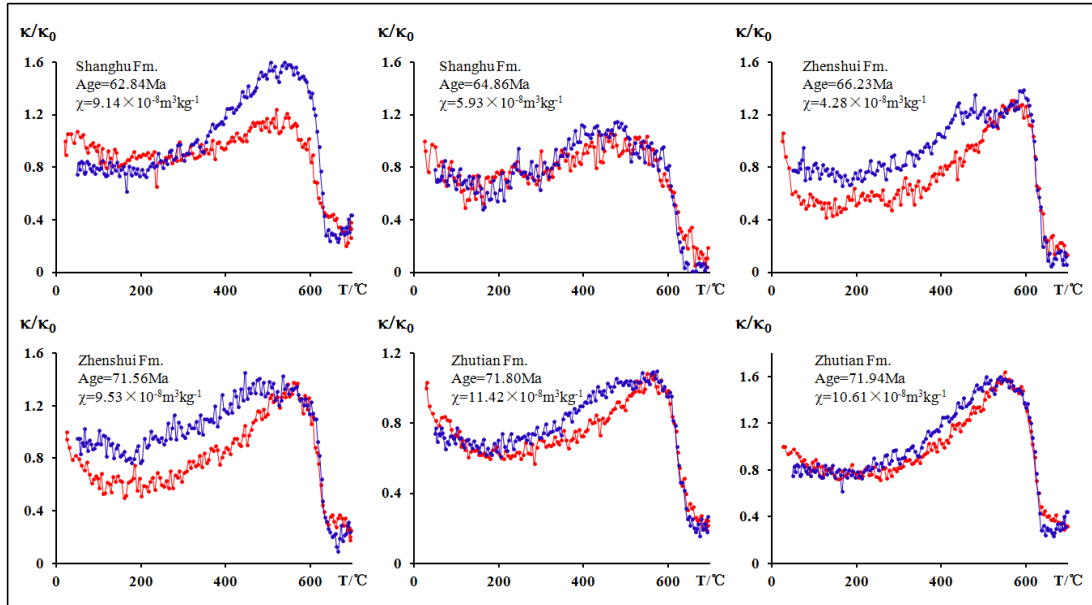
Fig. 3 The κ-T curves of pilot samples from the Datang Profile (red lines represent heating curves, whereas blue lines indicate cooling curves)

3.3 χ, SIRM, HIRM, and B_{cr}

The χ values are controlled by the types, concentrations, and particle sizes of magnetic minerals in the samples; all ferromagnetic, ferrimagnetic, antiferromagnetic, and paramagnetic minerals have effects on χ. In contrast, SIRM, HIRM, and B_{cr} are not affected by paramagnetic minerals or superparamagnetic particles. Therefore, χ and SIRM can be used to indicate the concentration of magnetic minerals in cases where one magnetic mineral is dominant. HIRM can be used to indicate the concentration of hard magnetic minerals such as haematite. The value of B_{cr} can be used to indicate the ratio of hard to soft magnetic minerals (Thompson & Oldfield, 1986; Evans & Heller, 2003). As shown in Fig. 4, the values of χ, SIRM, and HIRM are low: χ varies from 1.67 to 19.14 $\times 10^{-8}$ m^3 kg^{-1} with an average value of 7.25 $\times$ 10^{-8} m^3 kg^{-1}; SIRM varies from 55.27 to 626.26 $\times 10^{-5}$ Am^2 kg^{-1} with an average value of 212.36 $\times 10^{-5}$ Am^2 kg^{-1}; HIRM varies from 24.42 to 341.87 $\times 10^{-5}$ Am^2 kg^{-1}

240 with an average value of 124.11×10^{-5} Am^2 kg^{-1}. In addition, the variation trends of

241 these three parameters are similar: high with clear fluctuations in the Zhutian

242 Formation, a sharply decrease from the Zhutian Formation to the Zhenshui Formation,

243 low values with numerous fluctuations in the Zhenshui Formation, an increase in the

244 Pingling Part of the Shanghu Formation, and an overall decease again with significant

245 variations in the Xiahui Part of the Shanghu Formation. The B$_{cr}$ values vary from 300

246 to 600 mT with an average value of 430 mT, which indicate the dominant role of hard

247 magnetic minerals.

248   In addition to haematite, there were significant amounts of paramagnetic

249 minerals in the samples, as shown in κ-T curves (Fig. 3); the presence of

250 paramagnetic minerals may affect χ when the overall value of χ is low. However,

251 SIRM and HIRM are not affected by paramagnetic minerals, and their variation trends

252 are similar to those of χ, which suggests that the variations of χ, SIRM, and HIRM

253 are mainly controlled by the concentration of haematite (Thompson & Oldfield, 1986).

254
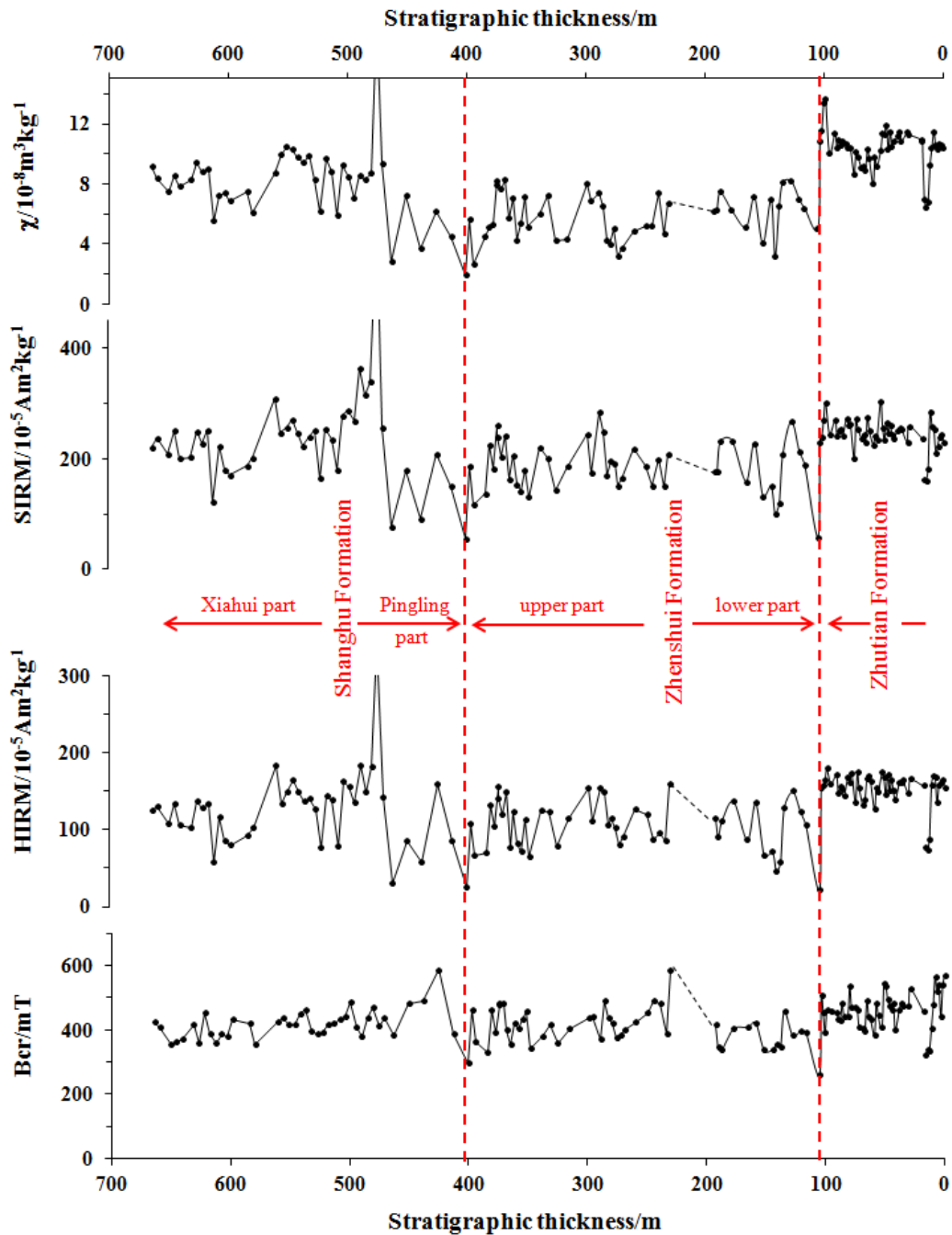
Fig. 4 Magnetic parameter variations of the Datang Profile; X axis indicates the stratigraphic thickness from the Zhutian Formation to the Shanghu Formation.

3.4 REEs

There are a variety of distribution patterns of REEs in different types of sediments because of their diverse origins and sources, and the evolution of the

260   palaeoenvironment. Therefore, REEs can be used as efficient tracer elements (Shunso

261   et al., 2010; Fagel et al., 2014). The ΣREE values of the Datang Profile samples vary

262   from 153.71 to 210.18 μg/g, with an average value of 183.28 μg/g. The REE

263   distribution patterns of the pilot samples nearly overlap (Fig. 5); these patterns are

264   characterised by a negative slope, moderate enrichment of LREEs, and a relatively

265   flat HREE pattern, as well as by a prominent negative Eu anomaly, which suggests

266   that the provenance of the red strata remained stable (Yan et al. 2007). These patterns

267   are consistent with those of eight samples from the Zhuguang and Qingzhang granites

268   (Shu et al., 2004), which indicates that they are closely related. However, the Eu

269   anomaly of the granites is more significant than those of the red strata, which is likely

270   related to post-depositional chemical weathering or mixing with other Cambrian–

271   Jurassic sediments (Shu et al., 2004).
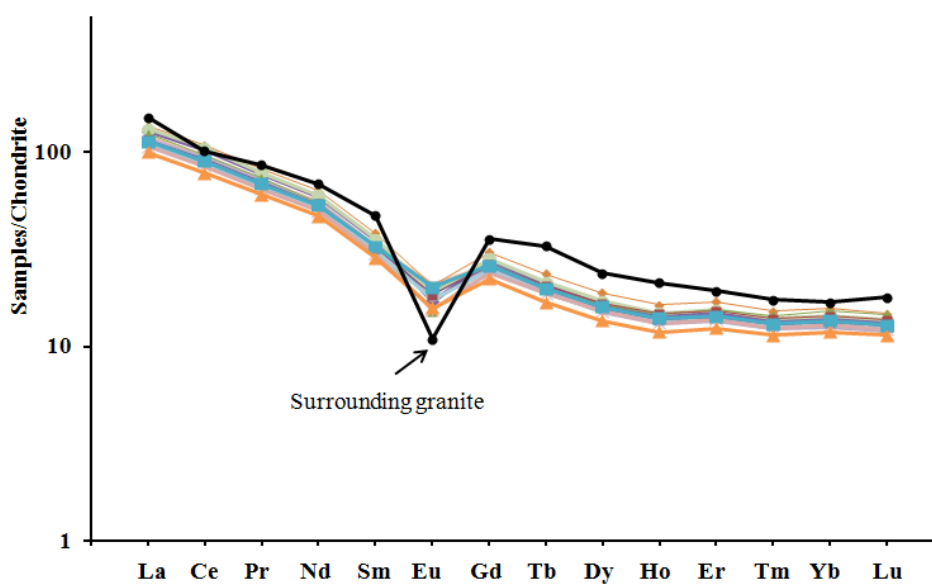
272

273

274   **Fig. 5** REE distribution patterns (normalised by chondrite) of pilot samples from the

275   Datang Profile and samples of the surrounding granite (average values of eight

276   samples, Shu et al., 2004)

277

4 Discussion

4.1 Chronological framework of the Datang Profile

A great deal of geochronology research, including palaeomagnetic, isotopic, and palaeontological studies, has been carried out on the Datang Profile (Zhao et al., 1991; Zhang et al., 2006; Clyde et al., 2010; Li et al., 2010; Tong et al., 2013). The most significant event recorded in this profile is the extinction of the non-avian dinosaurs and the subsequent evolutionary radiation of mammals, which indicate the end of the Cretaceous and the beginning of the Palaeogene (Zhao et al., 1991; Zhang et al., 2006; Clyde et al., 2010). Based on the palaeontological data and two basalt K–Ar ages (67.04 ± 2.34, 67.37 ± 1.49 Ma) from the top of the Yuanpu Formation (which corresponds to the Zhutian Formation in this paper), Zhao et al. (1991) suggested that the palaeomagnetic age of the Datang Profile is between 27R and 31R (Fig. 6A). However, Russell et al. (1993) challenged this chronology because of the wide variation of sedimentation rate, which varied by more than an order of magnitude during each chron, proposed an alternative (Fig. 6B), and suggested that several millions of years of deposition was absent from the lowermost part of Palaeocene record. However, there are some fundamental flaws in Russell et al.'s age model. First, a lack of exact ages for palaeomagnetic chron identification made the age model inconclusive. Secondly, based on field observations, no hiatus occurred between the Shanghu Formation and the Zhenshui Formation (Ye et al., 2000; Zhang et al., 2006). Thirdly, it is reasonable to assume that the sedimentary rate differed during different chrons in the Nanxiong Basin, as a continental basin (Ye et al., 2000). Moreover, two U–Pb ages (59.76 ± 0.78, 60.76 ± 0.90 Ma) of a tephra layer from the middle part of

the Nongshan Formation, above the Shanghu Formation, were recently obtained

(Tong et al., 2013), and confirm that the age model of Russell et al. was incorrect. To

further clarify the palaeomagnetism framework of the Datang Profile, Clyde et al.

(2010) collected samples from the uppermost 465 m of the Datang Profile (i.e. the

lower part of Zhenshui Formation and Shanghu Formation) and the DT05 profile

(Nongshan Formation and the lower part of Guchengcun Formation), and combined

the results with palaeontological data and δ^{13}C and δ^{18}O isotopic composition data

from palaeosol carbonates. The results show that the upper 465 m of the Datang

Profile has five well-defined polarity zones (30N, 29R, 29N, 28R, and 28N), whereas

the DT05 section is characterised by a single long, reversed-polarity zone (26R),

which has been confirmed by the U–Pb ages of the tephra layer from the Nongshan

Formation (Tong et al., 2013), and suggests that this chronological work is reasonable.

However, the ages of the Zhutian Formation to the upper part of Zhenshui Formation

remain unclear.
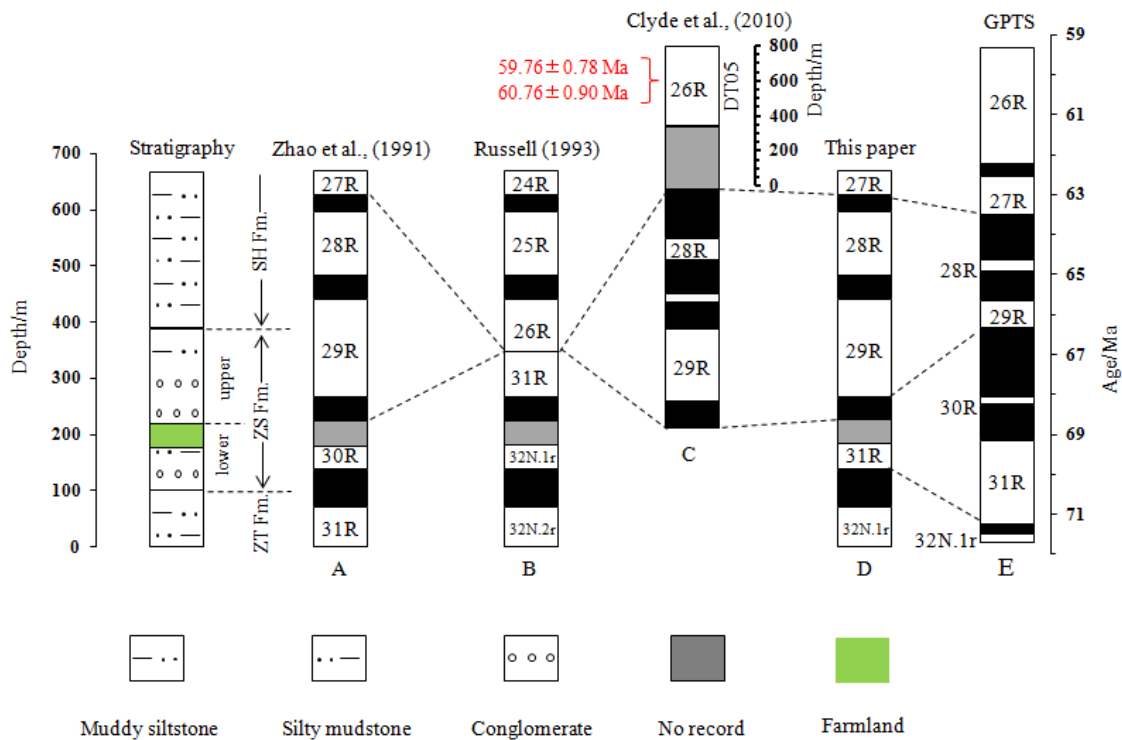
Fig. 6 Palaeomagnetic chronology framework of Datang Profile, A) Zhao et al., 1991; B) Russell et al., 1993; C) Clyde et al., 2010; D) this paper; E) Magnetic polarity time scale (Gradstein et al., 2012)

The age of the Zhutian Formation to the upper part of the Zhenshui Formation in Zhao's model is controversial; the basalts whose age was used for palaeomagnetic chron identification were actually intrusive rocks that formed after the Zhutian Formation was deposited, and therefore cannot be regarded as the top age of the Zhutian Formation. Thus, the top age of the Zhutian Formation should be older than 67.4 Ma (Zhang & Li, 2000), and it was confirmed with biostratigraphic data (*Tenuestheria*) that the Zhenshui Formation correlates with Maastrichtian formations, whereas the Zhutian Formation correlates with lower Santonian–Campanian formations (Li et al., 2010). Therefore, it was incorrect to use 67.4 Ma as the top age of the Zhutian Formation in Zhao's model. The Zhenshui Formation is predominantly composed of coarse clastic deposits, and the top 45.2 m of the lower part is covered in farmland (Fig. 1D and Fig. 6); therefore, it is not possible to obtain samples for palaeomagnetic analysis, which likely led to the absence of two short time chrons— 30R (0.173 Ma, Gradstein et al., 2012) and 31N (0.9 Ma, Gradstein et al., 2012)— from the palaeomagnetic results. Therefore, a new alternative can be proposed, as shown in Fig. 6D: 30R, 31N, and 31R in Zhao's model are modified to 31R, 32N.1n, and 32N.1r. The calculated boundary age of the Zhenshui and Zhutian Formations is ~71.5 Ma according to the new age model. This is slightly differ from the biostratigraphic age (~72.1Ma, i.e. the boundary age between Maastrichtian and Campanian), the reasons probably are 1) the samples for biostratigraphic age were collected from the whole Zhutian Formation that is more than 1000m in depth, while the Zhutian Formation in Datang Profile is just the top part of the whole Zhutian

341 Formation (Fig.1), and 2) the dereferences in sampling or time resolution between

342 these two dating methods; therefore, it is reasonable to cause a little error between

343 palaeomagnetic and biostratigraphic ages. If 72.1Ma (within C32N.2n) was regarded

344 as the boundary age of the Zhenshui and Zhutian Formations,then 30R (0.173 Ma),

345 31N (0.9 Ma), 31R (2.18Ma) and 32N.1n (0.24Ma) were missing due to the covered

346 farmland, and thus only 45.2m sediments deposited during more than 3.4Ma, which

347 seems unreasonable to have such a low sedimentary rate in this period. According to

348 the chronological framework obtained above, the bottom and top ages of the Datang

349 Profile can be calculated using linear extrapolation as 72 Ma and 62.8 Ma,

350 respectively.

351 **4.2 Sedimentary environment analysis**

352 Many aquatic fossils, such as ostracods and charophytes, were found in the red

353 strata, and there are many coarse sandstone and conglomerate layers; therefore, the

354 sediments were interpreted as fluvial or lacustrine facies in previous studies (Zhang et

355 al., 2006; Clyde et al., 2010; Wang et al., 2015). In greater detail, the Zhutian

356 Formation was regarded as floodplain and shallow lake deposits, the Zhenshui

357 Formation was interpreted as fluvial deltaic deposits, and the Shanghu Formation was

358 regarded as shallow lake deposits (Wang, 2012). However, there are dozens of

359 calcareous nodule layers (Fig. 7A and 7B), generated by pedogenic processes,

360 distributed in muddy sandstone and sandy mudstone layers (Clyde et al., 2010; Wang,

361 2012), especially in the Shanghu and Zhutian Formations. In addition to calcareous

362 nodules, other evidence for palaeosol formation was found, such as wormhole

363 remains (Fig. 7C and 7D), root traces (Fig. 7E) and obvious rhizoliths (Fig. 7F).

364 Moreover, many mud-cracks are observed in the Datang Profile (Figs. 7G and 7H).

365 Mud-cracks mainly form under alternating dry–wet environments, which have

366 traditionally been regarded as an indicator of arid or seasonally arid environments.

367 Environmental magnetic results (Figs. 3 and 4) show that haematite is the dominant

368 magnetic minerals in the red strata. Haematite is an iron oxide that mainly forms and

369 is preserved in oxidising environments, and will be dissolved or transformed under

370 excessively wet and reducing conditions. The widely distributed haematite and

371 palaeosols in the Datang Profile suggest that the sediments were exposed in a

372 relatively arid and oxidising environment.
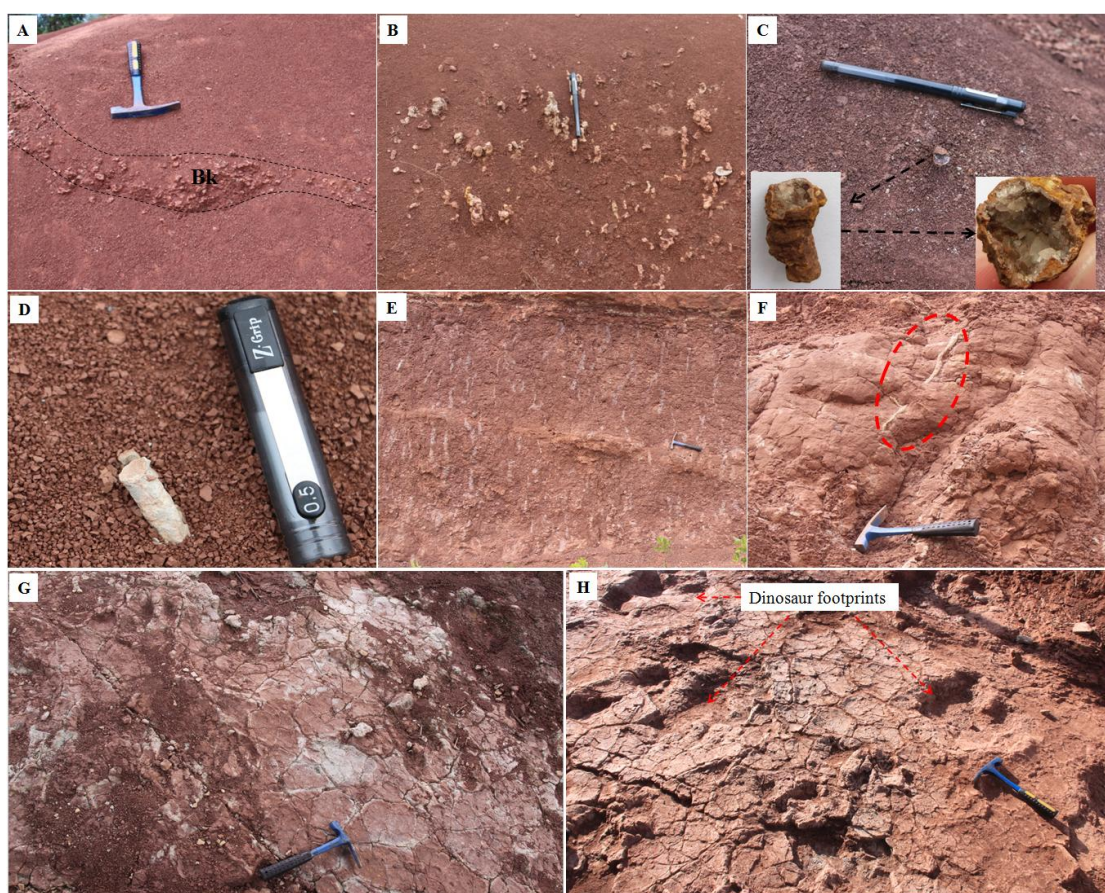
373

374   **Fig. 7** Evidence of palaeosols in the Datang Profile: calcareous nodule layers

375   generated during pedogenic processes (A and B), wormhole remains filled with

376 calcite (C) and grey mudstone (D), root traces (E) and obvious rhizolith (F), as well as

377   mud-cracks (G and F).

378   The climate during the Cretaceous represented one of the "greenhouse states" of

379   Earth history; the maximum CO_2 concentration was nearly 10 times higher and the

380   temperature 3–10℃ higher than those prior to the Industrial Revolution (Huber et al.,

381   2002; Wilson et al., 2002; Retallack, 2009). Although the CO_2 concentration

382   decreased in the Late Cretaceous, it was still higher than today (Wang et al., 2014,

383   and the references therein). The Nanxiong Basin was belonged to a hot and arid belt

384   according to the palaeoclimate classification of Chumakov et al. (2004). Clumped

385   isotope analysis of pedogenic carbonates has shown that the palaeotemperature could

386   reach up to 27.3–38.2℃, with an average value of 34℃ (Zhang, 2016), which

387   suggests that the temperature during the Late Cretaceous to Early Palaeocene was

388   much higher than that of the present in this area. In addition, the $CaCO_3$ contents are

389   10–20% (wt, Yang et al., 2007) in the red strata, and there are many pedogenic

390   carbonate layers in the sandy mudstone and muddy sandstone, which suggest that the

391   leaching process was weak and that rainfall was moderate (Retallack, 1999, 2005;

392   Yan et al., 2007). TOC concentration is very low (0.027–0.258 wt%, Yan et al., 2007),

393   which is likely related to the sparse vegetation coverage or oxidising conditions

394   unfavourable for TOC preservation. Therefore, all geochemical parameters indicate

395   that the overall climate during the Late Cretaceous to Early Palaeocene in the

396   Nanxiong Basin was tropical (semi-) arid.

397   Therefore, the depositional processes of red strata in the Nanxiong Basin under

398   (semi-) arid climate conditions can be inferred as follows. Weathered materials were

399   transported from the surrounding area by runoff caused by rainfall and were then

400   deposited in the basin. During the interval with greater rainfall, temporary rivers or

401   lakes appeared in the basin and provided a habitat for the low-level aquatic organisms

402   such as ostracods and charophytes, and left abundant fossils of these organisms in the

strata. However, the rivers or lakes could not persist for long in a hot, (semi-) arid

climate; after the weathered materials were deposited in the basin, these temporary

rivers and lakes disappeared because of strong evaporation, and the sediments were

then exposed to an oxidising environment. Haematite was thus generated, and the

organic matter rapidly decomposed, which led to very low TOC values (Yan et al.,

2007). Pedogenic processes then developed, and moderately to fully mature soils with

diagnostic characters such as Bk horizons, wormholes and root traces formed in sandy

mudstone and muddy sandstone layers. No typical palaeosols were found in the

coarse sandstone or conglomerate layers in the Zhenshui Formation because of the

lack of essential conditions for soil formation, but many root traces were preserved

(Figs. 7E and 7F), which can be called "weakly developed soils".

4.3 Comparison between χ and $\delta^{18}O$, and the corresponding mechanism

At present, most high-resolution records of palaeoclimate changes during the

Late Cretaceous to Early Palaeogene were derived from marine sediments, with few

from continental sediments, which has limited comparison between marine records

and continental records and even the study of the dynamic mechanism of

palaeoclimate evolution (Wang et al., 2013b). The $\delta^{18}O$ values of benthic foraminifera

in marine sediments faithfully recorded global palaeotemperature changes over the

past 200 Ma (Zachos et al., 2001; Friedrich et al., 2012; Bodin et al., 2015), which has

provided a high-resolution reference for the study of continental records (Fig. 8A). As

shown in Fig. 8, there is a significant negative correlation between χ and $\delta^{18}O$ for the

Pacific and South Atlantic (Friedrich et al., 2012) from 72 Ma to 62.8 Ma: high (low)

χ values correlate with low (high) $\delta^{18}O$ values, which suggest that χ values likely

recorded the global palaeoclimate evolution.

427
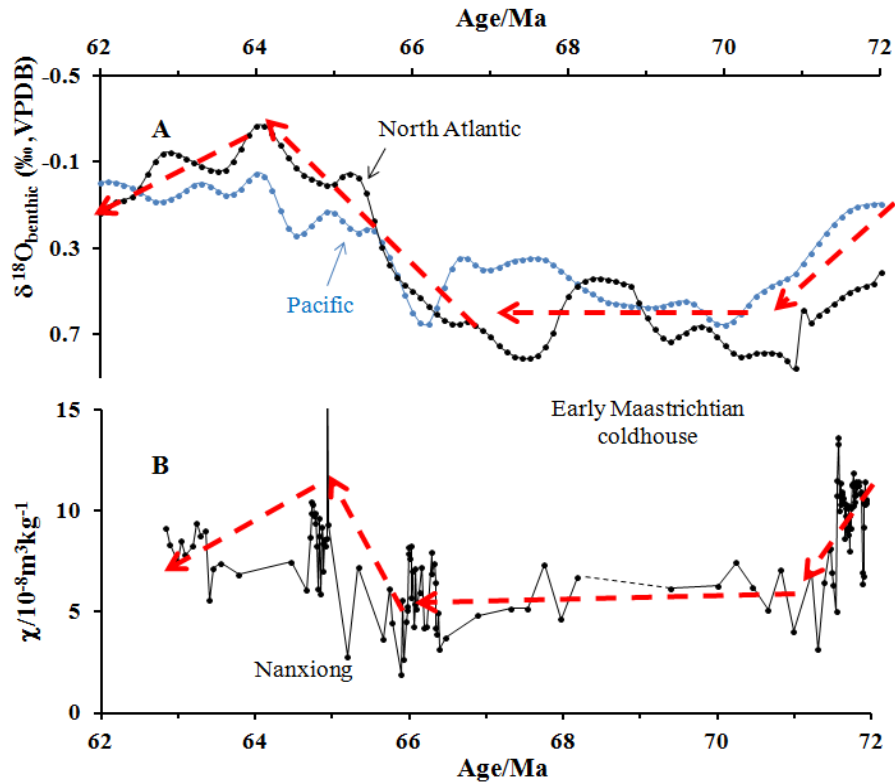
Fig. 8 Correlations between $\delta^{18}O$ from Pacific and North Atlantic records (A) and

χ from the Datang Profile (B) from 72 Ma to 62.8 Ma; higher $\delta^{18}O$ values correlate

with lower χ values

The parameter χ has been widely applied in Chinese Quaternary loess–palaeosol

and Tertiary red clay sequences as an efficient palaeoclimatic indicator, and correlates

well with the $\delta^{18}O$ values of marine records (Liu, 1985; Nie et al., 2008). Multiple

glacial–interglacial cycles occurred during the Quaternary, and the climate during

interglacial periods was warmer and more humid than that of glacial periods, which

led to the formation of palaeosols. Palaeosols are magnetically enhanced because of

in-situ pedogenic formation of magnetite and maghemite under elevated temperature

and rainfall conditions, which lead to higher χ values in palaeosol layers than in loess

layers in the Chinese Loess Plateau (CLP, Zhou et al., 1990; Liu et al., 1992; Maher et

al., 1994; Chen et al., 2005; Hao & Guo, 2005). The climate was warmer and more

441   humid during the Tertiary than in Quaternary interglacial periods, according to red

442   clay records (Ding et al., 1999, 2001), but most χ values of red clays were lower than

443   those of Quaternary palaeosols and even lower than those of loess layers (Nie et al.,

444   2008), which indicates that the pedogenic hypothesis cannot be simply applied in red

445   clay layers. The dominant magnetic minerals in loess are original magnetite and

446   haematite, with minor amounts of pedogenic maghemite. In contrast, in palaeosol

447   layers, the dominant magnetic minerals are pedogenic maghemite and magnetite, with

448   minor amounts of magnetite, and in red clay layers, the dominant magnetic minerals

449   are pedogenic haematite with minor pedogenic maghemite (Xie, 2008). As mentioned

450   above, the climate when the red clay layers formed was warmer and more humid, and

451   pedogenesis was stronger; consequently, a large amount of ultrafine strongly

452   magnetic minerals such as maghemite and magnetite formed (Nie et al., 2007, 2014,

453   2016). Previous studies have shown that low-temperature oxidation (LTO) of

454   magnetite is a common process during weathering (VanVelzen & Dekkers, 1999) that

455   gradually alters magnetite into maghemite (magnemitisation). Moreover, chemical

456   weathering can transform maghemite into haematite (Sidhu, 1988; Torrent et al., 2006;

457   Zhang et al., 2012; Fang et al., 2015; Hu et al., 2015). The magnetic minerals in red

458   clays underwent stronger oxidation than Quaternary loess–palaeosol sequences (Nie

459   et al., 2016), which likely caused most soft magnetic minerals (magnetite and

460   maghemite) to transform into hard magnetic mineral-haematite under LTO and

461   chemical weathering processes, and led to a significant decrease of χ values in red

462   clay. Nonetheless, χ values of red clay can still be used as an efficient palaeoclimatic

463   indicator (Nie et al., 2008; Zhao et al., 2016).

464   Generally, palaeosols, even without burial or original gleisation in deep time,

465   have systematically lower χ, such as observed for Precambrian and Palaeozoic

466   palaeosols (Retallack et al., 2003). Two possible explanations for this finding have

467   been proposed: 1) recrystallisation and metamorphism of magnetite and maghemite

468   (Retallack, 1991), and 2) lower biological productivity of such deeply buried and

469   ancient soils (Schwartzmann and Volk, 1991). However, these two possibilities

470   require further testing of palaeosols with a wider range of geological ages and degrees

471   of burial alteration (Retallack et al., 2003). Despite the low values of χ in many of

472   these deep time palaeosols, many studies have concluded that the magnetic minerals

473   preserved in these soils are pedogenic (Rankey and Farr, 1997; Cogoini et al., 2001;

474   Tramp et al., 2004). Therefore, we propose another possibility to explain the low χ in

475   the Nanxiong red strata. The global climate during the Late Cretaceous to Early

476   Palaeocene was much warmer than that of the Neogene and Quaternary (Friedrich et

477   al., 2012; Bodin et al., 2015). The Chemical Index of Alteration (CIA) values of red

478   strata in the Nanxiong Basin (70–80, Yan et al., 2007) are higher than those of

479   Quaternary loess–palaeosol and Tertiary red clay (61–71, Chen et al., 2001; Xiong et

480   al., 2010), which suggests that the red strata underwent stronger chemical weathering.

481   The climate during the Late Cretaceous to Early Palaeocene in the Nanxiong Basin

482   was hot and (semi-) arid, with a certain amount of rainfall, as represented by the

483   presence of temporary rivers and shallow lakes (or low-lying land) and palaeosols

484   with calcareous nodules (Retallack, 1999, 2005), which favoured the LTO of

485   magnetite and the transformation of maghemite to haematite through chemical

486   weathering, caused haematite to be the main magnetic mineral in the red strata (Figs.

487   2 and 3) and significantly decreased χ. This process is summarised in Fig. 9. The

488   global climate was unstable from 72 Ma to 62.8 Ma, as represented by multiple cycles

489   of cold/warm changes (Fig. 8A). Higher χ values occurred in warmer periods (lower

490    $\delta^{18}O$ values), which is similar to the correlation between the χ values of Chinese

491 loess–palaeosol/red clay successions and $\delta^{18}O$ (Liu, 1985; Nie et al., 2008). There

492 may be two reasons for the changes in χ : 1) changes of sediment provenance, and 2)

493 palaeoclimatic evolution. REE distribution patterns show that the sediment

494 provenance remained similar in the Datang Profile (Fig. 4), and even across the whole

495 basin (Yan et al., 2007), which indicates that palaeoclimatic evolution was the main

496 reason for changes in χ. There are significantly positive correlations between χ, SIRM,

497 and HIRM (Fig. 4), which suggest that χ was controlled by the concentration of

498 haematite (Figs. 3 and 4), whereas haematite was generated through LTO and

499 chemical weathering during pedogenesis. Thus, the relationship between χ and

500 haematite content can be explained by the "pedogenic-plus hypothesis": more

501 haematite formed during warmer and wetter periods with stronger pedogenesis, and

502 caused a higher χ, and opposite conditions yielded lower χ values. The similarity of

503 the χ and $\delta^{18}O$ curves suggests that the climate changes in the Nanxiong Basin during

504 72–62.8 Ma were similar to global trends; therefore, χ can still be used as an efficient

505 indicator for palaeoclimate changes in this basin.

506
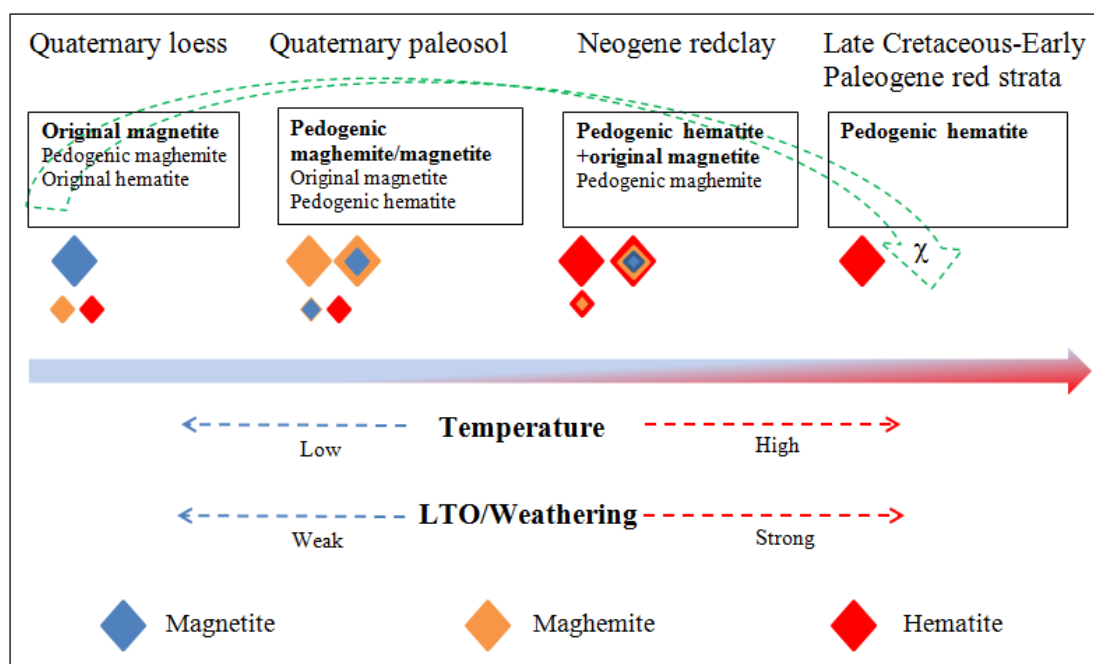
508   **Fig. 9** Cartoon illustrating the dominant magnetic minerals and χ changes from

509   Quaternary loess–palaeosol (CLP)→Neogene red clay (CLP)→Upper Cretaceous–

510   Lower Palaeogene red strata in Nanxiong Basin along with the increased temperature

511   and LTO/chemical weathering (the size of the symbols means the contribution to

512   χ but not the real size of magnetic particles).

513   Hasegawa et al., (2012) found that the subtropical high-pressure belt was located

514   between ca. 31°N and 37°N during the Late Cretaceous based on spatio-temporal

515   changes in the latitudinal distribution of deserts in the Asian interior, thus the

516   Nanxiong Basin (~20°N, Scotese, 2014) was out of the area covered by subtropical

517   high-pressure belt. Besides, computer simulation results revealed that the prevailing

518   wind directions showed a remarkable seasonal variation over East Asia at 66Ma,

519   which indicates a monsoon feature over East Asia at that time (Chen et al., 2013), and

520   even more remarkable compared to the present day, this was supported by the

521   geological evidences (Jiang et al., 2008), rainfall also showed a seasonal variation

522   between dry and wet seasons corresponding to the monsoon (Chen et al., 2013). In

523   addition, the root traces in Zhenshui Formation consisting of elongate gray mottles

524   with red or purple hypocoatings (Fig. 7E) indicate a relatively well-drained soil

525   condition (Krous et al., 2006), which is favourite for the formation and preservation of

526   haematite. Therefore, the monsoon system already existed and the rainfall also

527   showed seasonal variation across the Cretaceous–Palaeogene boundary, but the

528   climate was more hotter and drier than present, so a great deal of haematite generated

529   during pedogenic processes under well-drained condition, and thus recorded the

530   global climate evolutions.

4.4 Palaeoclimatic evolution of the Nanxiong Basin during 72–62.8 Ma

Based on changes of the relative content of clay, the ratio of feldspar to quartz (F/Q) and the $\delta^{18}O$ of pedogenic carbonates, Wang et al. (2012, 2015) divided the palaeoclimatic changes recorded in the Datang Profile into three stages: an arid to semi-arid climate from the Zhutian Formation to the bottom of the Pingling part of the Shanghu Formation, a semi-arid to hot and humid climate from the bottom of the Pingling part to the bottom of the Xiahui part of the Shanghu Formation, and the semi-arid climate of the Xiahui part. Their age model follows the palaeomagnetic framework of Zhao et al. (1991, Fig. 6A). In contrast, Yan et al. (2007) suggested that a long period of extremely dry climate occurred in the Late Cretaceous, and that the climate then became relatively wet in the Early Palaeocene, based on $CaCO_3$ and TOC contents as well as the ratios of Rb/Ti and Cs/Ti. Furthermore, quantitative palaeotemperature data have been successfully determined; for example, clumped isotope analysis of pedogenic carbonates revealed that the palaeotemperature reached up to 27.3–38.2℃ with an average value of 34℃ (Zhang, 2016). Although a considerable amount of work has been conducted on these palaeoclimatic changes, the reconstructed results cannot be compared efficiently with global records. One reason may be the low resolution of quantitative palaeotemperature data due to the limitations of sampling (e.g. pedogenic carbonates), and another may be that the geochronological framework is incorrect (section 4.1). As shown in previous studies, the $\delta^{18}O$ of pedogenic carbonates was found to be an efficient palaeotemperature indicator in terrestrial sediments; greater $\delta^{18}O$ values indicate higher palaeotemperatures (Han et al., 1997; Chamberlain et al., 2012; Gao et al., 2015). In addition, the haematite in the Nanxiong Basin is partially Al-substituted (Fig. 3); indoor examination revealed that there was a negative correlation between T_N and the

556 Al content of Al-substituted haematite (Jiang et al., 2012), and greater Al content in

557 haematite likely indicates stronger pedogenesis. Therefore, we combined these results

558 with the χ curve, $\delta^{18}O$ of pedogenic carbonates (Fig. 10B, Clyde et al., 2010; Wang,

559 2012), and T_N of the pilot samples (Fig. 10C) to reconstruct the climatic evolution of

560 the Nanxiong Basin during 72 to 62.8 Ma.
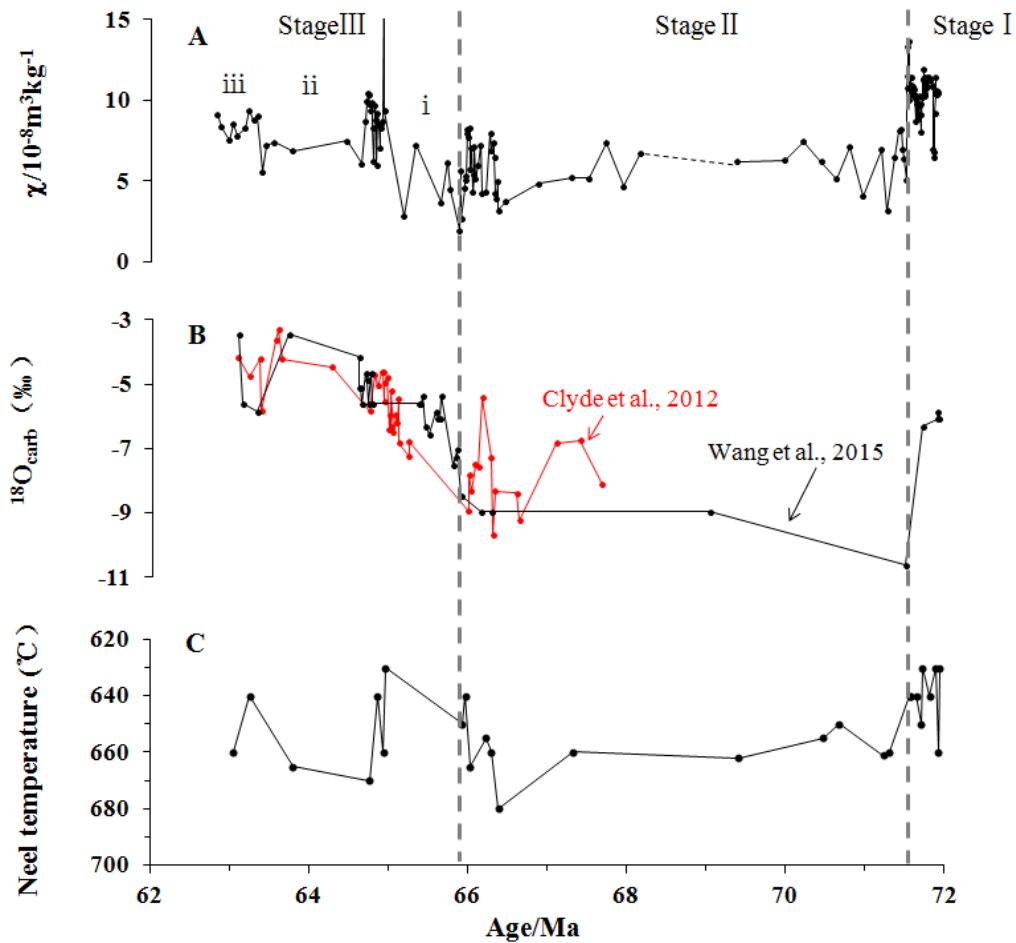
561

562 **Fig. 10** Combined proxies for palaeoclimatic changes in the Nanxiong Basin from 72

563 to 62.8 Ma, A) χ curve, B) $\delta^{18}O$ of pedogenic carbonates (Clyde et al., 2010; Wang,

564 2012), and C) T_N of Al-substituted haematite of pilot samples

565 Although the palaeoclimate from 72 to 62.8 Ma in the Nanxiong Basin was

566 overall hot and (semi-) arid, it can be divided into three stages, as shown in Fig. 10.

567 For stage I (from 72 to 71.5 Ma, Zhutian Formation), χ and $\delta^{18}O$ values of pedogenic

568 carbonates are relatively high, and T_N is relatively low and varies from 630 to 660℃

569 with a mean value of 640℃, whereas the $\delta^{18}O$ values of marine sediments are

570 relatively low (Fig. 8); the sediments are mainly composed of muddy siltstone and

571 silty mudstone (shallow lake facies), which indicate a relatively hot and wet climate

572 with stronger pedogenic processes and clear fluctuations, such as the rapid drying and

573 cooling event at ~71.7 Ma, represented by low χ values. In stage II (from 71.5 to 66

574 Ma, Zhenshui Formation), χ decreases sharply at 71.5 Ma and then fluctuates steadily,

575 $\delta^{18}O$ values of pedogenic carbonates show a similar trend to χ, T_N is relatively high

576 and varies from 640 to 680℃ with a mean value of 660℃, $\delta^{18}O$ of marine sediments

577 first increases and then fluctuates at a high level, and the sediments are mainly

578 composed of coarse sandstone and conglomerate (fluvial delta facies), which indicate

579 a relatively cool and arid climate with weak pedogenesis; these findings are supported

580 by sparse pollen data that show the appearance of the Pinaceae and disappearances of

581 tropical plants in the upper Zhenshui Formation, which indicate a cold climate (Erben

582 et al., 1995). In Stage III (from 66 to 62.8 Ma, Shanghu Formation): χ increases

583 sharply from 66 to ~64.7 Ma, then decreases sharply at 64.7 Ma, and maintains

584 relative low values from 64.7 to ~63.4 Ma, and then returns high values from 63.4 to

585 62.8 Ma; $\delta^{18}O$ values of pedogenic carbonates increase rapidly from 66 to ~64.7 Ma

586 and then maintain high values from 64.7 to ~62.8 Ma; T_N of pilot samples and $\delta^{18}O$ of

587 marine sediments show opposite trends from χ; the sediments from 66–62.8 Ma are

588 mainly composed of muddy siltstone and silty mudstone (shallow lake facies). In

589 addition, sparse pollen analyses have shown that the climate was temperate–

590 subtropical at the bottom of the Pingling part (~66 to ~65 Ma) (Li, 1989), whereas it

591 was cool and arid in the Xiahui part (Zhang et al., 1981); therefore, the climate

592 changes in this stage can be divided into three sub-stages: in sub-stage i (66–64.7 Ma),

593 the climate quickly became relatively hot and wet from relatively cool and arid

594 conditions; in sub-stage ii (64.7–63.4 Ma), the climate was relatively drying and

595 cooling event represented by low χ values; in sub-stage iii (63.4–62.8 Ma), the

596 climate became relatively hot and wet again. Although the constructed climate

597 evolution revealed by magnetic parameters is still qualitative, it shows more details

598 than other proxies or the marine record, such as the several sub-fluctuations during

599 each stage, which probably indicates that the climate changes from 72 to 62.8 Ma

600 were probablyly instable with more fluctuations, and this needs our further work to

601 provide quantitative and higher resolution results in the future.

602 **5 Conclusions**

603 1. Some defects have been identified in the previous palaeomagnetic

604 chronological frameworks because of the lack of reliable control ages for

605 identification of palaeomagnetic chrons. Combined with the most recently published

606 isotopic ages of volcanic ash and biostratigraphic dating, a new chronological

607 framework has been proposed; the results show that the age of the Datang Profile is

608 between 72 to 62.8 Ma.

609 2. Many aquatic fossils, such as ostracods and charophytes, were found in the red

610 strata, and the sediments were interpreted as fluvial or lacustrine facies; however,

611 haematite is the dominant magnetic mineral throughout the profile, and furthermore,

612 palaeosol layers, pedogenic carbonates, wormhole remains, root traces, clear

613 rhizoliths and mud-cracks were found, which indicate that those rivers or lakes, if

614 present, appeared only temporarily in these hot and (semi-) arid environments, such

that the sediments were exposed to (semi-) arid and oxidising condition for long periods of time and experienced different degrees of pedogenesis.

3. The variations of χ were controlled by the concentration of haematite, which was generated through LTO and chemical weathering during pedogenesis in hot and (semi-) arid environment. Moreover, the stronger the pedogenic processes, the more haematite was generated, and the higher the χ values.

4. The χ curve of the Datang Profile is similar to the $\delta^{18}O$ curves of corresponding marine sediments, which suggests that climate changes in the Nanxiong Basin during 72–62.8 Ma were similar to global trends, and can be divided into three stages: 1) a relatively hot and wet climate from 72 to 71.5 Ma with a rapid drying and cooling event at ~71.7 Ma; 2) a relatively cool and arid climate with secondary fluctuations from 71.5 to 66 Ma; and 3) a relatively hot and wet climate again from 66 to 62.8 Ma, which can be divided into 3 sub-stages: i) the climate quickly became hot and wet from 66 to 64.7 Ma, ii) a notable drying and cooling event at 64.7–63.4 Ma, and iii) a relatively hot and wet climate from 63.4 to 62.8 Ma.

Author contribution: Mingming Ma and Xiuming Liu designed the experiments and Wenyan Wang carried them out. Mingming Ma prepared the manuscript with contributions from all co-authors.

Competing interests: The authors declare that they have no conflict of interest.

Acknowledgement: The authors thank Xianqiu Zhang (China New Star (Guangzhou) Petroleum Corporation) for his generous help in field work. This research was supported by National Science Foundation of China (Grant Nos. 41210002, 41602185 and U1405231), Natural Science Foundation of Fujian Province (Grant No. 2016J05095), and Non-Profit Research Funds of Fujian Province (Grant No. 2016R10323).

640

References

Balsam, W. L., and Deaton, B. C., 1991. Sediment dispersal in the Atlantic Ocean—evaluation by visible-light spectra, Rev. Aquat. Sci. 4, 411 –447.

Balsam, W., Ji,J. F., Chen, J., 2004. Climatic interpretation of the Luochuan and Lingtai loess sections, China, based on changing iron oxide mineralogy and magnetic susceptibility, Earth Planet. Sci. Lett. 223, 335–348

Barrera, E., Savin, S.M., 1999. Evolution of late Campanian-Maastrichtian marine climates and oceans. In: Barrera, E., Johnson, C. (Eds.), Evolution of the Cretaceous Ocean-Climate System. Geol. Soc. Am. Spec. Pap. 332, 245-282.

Bechtel, A., Jia, J., Strobl, S.A.I., Sachsenhofer, R.F., Liu, Z., Gratzer, R., Püttmann, W., 2012. Palaeoenvironmental conditions during deposition of the Upper Cretaceous oil shale sequences in the Songliao Basin (NE China): Implications from geochemical analysis. Org. Geochem. 46, 76-95.

Bodin, S., Meissner, P., Janssen, N.M.M., Steuber, T., Mutterlose, J., 2015. Large igneous provinces and organic carbon burial: Controls on global temperature and continental weathering during the Early Cretaceous. Global Planet. Change. 133, 238-253.

Buck, B.J., Hanson, A.D., Hengst, R.A., Hu, S.2004. "Tertiary Dinosaurs" in the Nanxiong Basin, Southern China, Are Reworked from the Cretaceous. J. Geol. 112(1), 111-118.

Chamberlain, C. P., Mix, H. T., Mulch, A., Hren, M. T., Kent-Corson, M. L., Davis, S. J., Horton, T. W., Graham, S. A., 2012. The Cenozoic climatic and topographic evolution of the western North American Cordillera. Am. J. Sci. 312(2), 213-262.

Chamberlain, C.P., Wan, X., Graham, S.A., Carroll, A.R., Doebbert, A.C., Sageman, B.B., Blisniuk, P., Kent-Corson, M.L., Wang, Z., 2013. Stable isotopic evidence for climate and basin evolution of the Late Cretaceous Songliao basin, China. Palaeogeogr. Palaeoclimatol. Palaeoecol. 385(3), 106-124.

Chen, J., An, Z., Liu, L., Ji, J., Yang, J., Chen, Y. 2001. Variations in chemical compositions of the eolian dust in Chinese Loess Plateau over the past 2.5 Ma and chemical weathering in the Asian inland. Sci. China Earth Sci. 44(5), 403-413.

Chen, J., Zhao, P., Wang, C., Huang, Y., Cao, K., 2013. Modeling East Asian climate and impacts of atmospheric CO_2 concentration during the late Cretaceous (66 Ma). Palaeogeogr. Palaeoclimatol. Palaeoecol. 385(9), 190-201.

Chen, T., Xu, H., Xie, Q., Chen, J., Ji, J. Lu, H., 2005. Characteristics and genesis of maghemite in Chinese loess and paleosols: mechanism for magnetic susceptibility enhancement in paleosols, Earth planet. Sci. Lett., 240(3–4), 790–802.

Chumakov, N.M. Climatic zones and climate of the Cretaceous period, in: Semikhatov, M.A., Chumakov, N.M. (Eds.), Climate in the epochs of major biospheric transformations. Transactions of the Geological Institute of the Russian Academy of Sciences, 2004, 105-123.

Clyde, W.C., Ting, S., Snell, K.E., Bowen, G.J., Tong, Y., Koch, P.L., :I, Q., Wang, Y., 2010. New Paleomagnetic and Stable-Isotope Results from the Nanxiong Basin, China: Implications for the K/T Boundary and the Timing of Paleocene Mammalian Turnover. J. Geol. 118(2), 131-143.

Cogoini, M., Elmore, R.D., Soreghan, G.S., Lewchuk, M.T., 2001. Contrasting rock-magnetic characteristics of two Upper Paleozoic loessite‐paleosol profiles. Phys. Chem. Earth Solid Earth Geod. 26, 905–910.

Cramer, B.S., Toggweiler, J.R., Wright, J.D., Katz, M.E., Miller, K.G., 2009. Ocean overturning since the late cretaceous: inferences from a new benthic foraminiferal isotope compilation. Paleoceanography. 24(4), 43-47.

Ding, Z.L., Sun, J.M., Yang, S.L., Liu, T.S., 2001. Geochemistry of the pliocene red clay formation in the Chinese Loess Plateau and implications for its origin, source provenance and paleoclimate change. Geochim. Cosmochim. Ac. 65(6), 901-913.

Ding, Z.L., Xiong, S.F., Sun, J.M., Yang, S.L., Gu, Z.Y., Liu, T.S., 1999. Pedostratigraphy and paleomagnetism of a ~7.0 Ma eolian loess–red clay sequence at Lingtai, Loess Plateau, north-central China and the implications for paleomonsoon evolution. Palaeogeogr. Palaeoclimatol. Palaeoecol. 152(1–2), 49-66.

695   Erben, H.K., Ashraf, A.R., Böhm, H., Hahn, G., Hambach, U., Krumsiek, K., Stets, J., Thein, J.,
696   Wuster, P., 1995. Die Kreide/Tertiär-Grenze im Nanxiong-Becken (Kontinentalfazies,
697   Südostchina). Erdwissenschaftliche Forschung 32, 245.
698   Evans, M.E., Heller, F., 2001. Magnetism of loess/palaeosol sequences: recent developments.
699   Earth Sci. Rev. 54, 129-144.
700   Evans, M.E., Heller, F., 2003, Environmental magnetismprinciples and applications of
701   environmagnetics. Acdemic Press.
702   Fagel, N., Allan, M., Roux, G.L., Mattielli, N., Piotrowska, N., Sikorski, J., 2014. Deciphering
703   human–climate interactions in an ombrotrophic peat record: REE, ND and Pb isotope
704   signatures of dust supplies over the last 2500 years (Misten bog, Belgium). Geochim.
705   Cosmochim. Ac. 135(7), 288-306.
706   Fang, X., Zan, J., Appel, E., Lu, Y., Song, C., Dai, S., 2015. An Eocene–Miocene continuous rock
707   magnetic record from the sediments in the Xining Basin, NW China: indication for Cenozoic
708   persistent drying driven by global cooling and Tibetan Plateau uplift. Geophys. J. Int. 201(1),
709   78-89.
710   Friedrich, O., Norris, R.D., Erbacher, J. 2012. Evolution of middle to Late Cretaceous oceans—A
711   55 m.y. record of Earth's temperature and carbon cycle. Geology. 40, 107-110.
712   Fu, C., Bloemendal, J., Qiang, X., Hill, M.J., An, Z., 2015. Occurrence of greigite in the Pliocene
713   sediments of Lake Qinghai, China, and its paleoenvironmental and paleomagnetic
714   implications. Geochem. Geophy. Geosy. 16(5), 1293-1306.
715   Gao, Y., Ibarra, D. E., Caves, J. K., Wang, C., Caves, J. K., Chamberlain, C. P., Graham, S. A.,
716   Wu, H., 2015. Mid-latitude terrestrial climate of East Asia linked to global climate in the
717   Late Cretaceous. Geology, 43(4),287-290.
718   Gradstein, F.M., Ogg, J.G., Schmitz, M.D., Ogg, G.M., 2012. The geologic time scale. Elsevier.
719   Han, J., Keppens, E., Liu, T., Paepe, R., Jiang, W., 1997. Stable isotope composition of the
720   carbonate concretion in loess and climate change. Quatern. Int. 37(2), 37-43.
721   Hao, Q. Z., Oldfield, F., Bloemendal, J., Guo, Z. T., 2008. A preliminary study of the magnetic
722   properties of loess and palaeosol samples from the Chinese Loess Plateau spanning the last
723   22 million years. Palaeogeogr. Palaeoclimatol. Palaeoecol. 260(3), 389-404.
724   Hao, Q., Guo, Z., 2005. Spatial variations of magnetic susceptibility of Chinese loess for the last
725   600 kyr: implications for monsoon evolution. J. Geophys. Res.-Solid Earth, 110, B12101,
726   doi:10.1029/2005JB003765.
727   Hasegawa, H., Tada, R., Jiang, X., Suganuma, Y., Imsamut, S., Charusiri, P., Ichinnorov, N.,
728   Khand, Y., 2011. Drastic shrinking of the Hadley circulation during the mid-Cretaceous
729   supergreenhouse. Clim. Past. 8, 1323-1337.
730   Hay, W.W., 2011. Can humans force a return to a 'Cretaceous' climate? Sediment. Geol. 235,
731   5-26.
732   Hu, S., Goddu, S.R., Herb, C., Appel, E., Lleixner, G., Wang, S., Yang, X., Zhu, X., 2015.
733   Climate variability and its magnetic response recorded in a lacustrine sequence in Heqing
734   basin at the SE Tibetan Plateau since 900 ka. Geophys. J. Int. 2015, 201(1), 444-458.
735   Huang, C., Retallack, G.J., Wang, C., Huang, Q., 2013. Paleoatmospheric pCO_2, fluctuations
736   across the Cretaceous–Tertiary boundary recorded from paleosol carbonates in NE china.
737   Palaeogeogr. Palaeoclimatol. Palaeoecol. 385(3), 95-105.
738   Huang, C.M., Retallack, G.J., Wang, C.S., 2012. Early Cretaceous atmospheric pCO_2 levels
739   recorded from pedogenic carbonates. Cretaceous Res. 33, 42-49.
740   Huber, B.T., Hodell, D.A., Hamilton, C.P., 1995. Mid- to Late Cretaceous climate of the southern
741   high latitudes: stable isotopic evidence for minimal equator-to-pole thermal gradients. Geol.
742   Soc. Am. Bull. 107, 392-417.
743   Huber, B.T., Norris, R.D., Macleod, K.G., 2002. Deep-sea paleotemperature record of extreme
744   warmth during the Cretaceous. Geology. 30(2), 123-126.
745   Ji, J. F., Balsam, W., Chen, J., 2001. Mineralogic and climatic interpretations of the Luochuan
746   loess section (China) based on diffuse reflectance spectrophotometry, Quat. Res. 56, 23– 30,
747   Ji, J., Zhao, L., Balsam, W., Chen, J., Wu, T., Liu, L., 2006. Detecting chlorite in the Chinese
748   loess sequence by diffuse reflectance spectroscopy. Clay. Clay Miner. 54(2), 266-273.
749   Jiang, X., Pan, Z., Xu, J., Li, X., Xie, G., Xiao, Z., 2008. Late Cretaceous aeolian dunes and
750   reconstruction of palaeo-wind belts of the Xinjiang Basin, Jiangxi province,
751   China. Palaeogeogr. Palaeoclimatol. Palaeoecol. 257(1), 58-66.

Jiang, Z., Liu, Q., Barrón, V., Torrent, J., Yu, Y., 2012. Magnetic discrimination between Al-substituted hematites synthesized by hydrothermal and thermal dehydration methods and its geological significance. J. Geophys. Res.-Solid Earth, 117 (B2), 119-130.

Jiang, Z., Liu, Q., Zhao, X., Jin, C., Liu, C., Li, S., 2015. Thermal magnetic behaviour of Al-substituted haematite mixed with clay minerals and its geological significance. Geophys. J. Int. 200(1), 130-143.

Kraus, M. J., Hasiotis, S. T., 2006. Significance of different modes of rhizolith preservation to interpreting paleoenvironmental and paleohydrologic settings: examples from paleogene paleosols, Bighorn Basin, Wyoming, U.S.A. J. Sediment. Res. 76(4), 633-646.

Larrasoaña, J.C., Roberts, A.P., Rohling, E.J., 2008. Magnetic susceptibility of eastern Mediterranean marine sediments as a proxy for Saharan dust supply? Mar. Geol. 254(3-4), 224-229.

Levy, D., Giustetto, R., Hoser, A., 2012. Structure of magnetite (Fe_3O_4) above the Curie temperature: a cation ordering study. Phys. Chem. Miner. 39(2), 169-176.

Li, G., Hirano, H., Batten, D.J., Wan, X., 2010, Biostratigraphic significance of spinicaudatans from the Upper Cretaceous Nanxiong Group in Guangdong, South China. Cretaceous Res. 31(4), 387-395.

Li, J., Wen, X.Y., Huang, C.M., 2015. Lower Cretaceous paleosols and paleoclimate in Sichuan Basin, China. Cretaceous Res. 62, 154-171.

Li, M., 1989. Sporo-pollen from Shanghu Formation of Early Paleocene in Nanxiong Basin, Guangdong. Acta Palaeontologica Sinica. 28 (6), 741-750. (in Chinese with English abstract)

Li, X., Xu, W., Liu, W., Zhou, Y., Wang, Y., Sun, Y., Liu, L., 2013. Climatic and environmental indications of carbon and oxygen isotopes from the Lower Cretaceous calcrete and lacustrine carbonates in Southeast and Northwest China. Palaeogeogr. Palaeoclimatol. Palaeoecol. 385(3), 171-189.

Li, Y.W., 1988. The Application of Ostracoda to the Location of the Non-marine Jurassic-Cretaceous Boundary in the Sichuan Basin of China. Developments in Palaeontology & Stratigraphy, 11, 1245-1260.

Linnert, C., Robinson, S.A., Lees, J.A., Bown, P.R., Pérez-Rodriguez, I., Petrizzo, M.R., Falzoni, F., Littler, K., Arz, J.A., Russell, E.E., 2014. Evidence for global cooling in the Late Cretaceous. Nat. Commun. 5, 4194.

Liu, Q.S., Deng, C.L., Yu, Y.J., Torrent, J., Jackson, M.J., Banerjee, S.K., Zhu, R., 2005. Temperature dependence of magnetic susceptibility in an argon environment: implications for pedogenesis of Chinese loess/palaeosols. Geophys. J. Int. 161, 102-112.

Liu, T.S., 1985. Loess and Environment. Beijing: Science Press. 1-481. (in Chinese)

Liu, X., Shaw, J., Liu, T., Heller, F., Yuan, B., 1992. Magnetic mineralogy of Chinese loess and its significance, Geophys. J. Int. 108(1), 301-308.

Liu, X.M., Hesse, P., Rolph, T., 1999. Origin of maghaemite in Chinese loess deposits: Aeolian or pedogenic? Phys. Earth Planet Inter. 112, 191-201.

Liu, X.M., Rolph, T., An, Z., Hesse, P., 2003. Paleoclimatic significance of magnetic properties on the Red Clay underlying the loess and paleosols in China. Palaeogeogr. Palaeoclimatol. Palaeoecol. 199(1-2), 153-166.

Lu, H.M., Meng, X.K., 2010. Morin Temperature and Néel Temperature of Hematite Nanocrystals. J. Phys. Chem. C. 114(49), 21291-21295.

Ma,M., Liu, X., Pillans, Brad J., Hu, S., Lü, B., Liu, H., 2013. Magnetic properties of Dashing Rocks loess at Timaru, South Island, New Zealand. Geophys. J. Int. 195, 75–85

Maher, B.A., 2016. Palaeoclimatic records of the loess/palaeosol sequences of the Chinese Loess Plateau. Quaternary Sci. Rev. 154, 23-84.

Maher, B.A., Possolo, A., 2013. Statistical models for use of palaeosol magnetic properties as proxies of palaeorainfall. Global Planet. Change. 111(12), 280-287.

Maher, B.A., Thompson, R., Zhou, L.P., 1994. Spatial and temporal reconstructions of changes in the Asian palaeomonsoon—a new mineral magnetic approach, Earth planet. Sci. Lett. 125, 461–471

Nie, J., King, J.W., Fang, X., 2007. Enhancement mechanisms of magnetic susceptibility in the Chinese red-clay sequence. Geophys. Res. Lett. 341(19), 255-268.

Nie, J., King, J.W., Fang, X., 2008. Link between benthic oxygen isotopes and magnetic susceptibility in the red‐clay sequence on the Chinese Loess Plateau. Geophys. Res. Lett.

809   35(3), 154-175.

810 Nie, J., Song, Y., King, J., 2016. A review of recent advances in red-clay environmental
811   magnetism and paleoclimate history on the Chinese Loess Plateau. Front. Earth Sci. 4: 27 doi:
812   10.3389/feart.2016.00027

813 Nie, J., Zhang, R., Necula, C., Heslop, D., Liu, Q., Gong, L., Banerjee, S., 2014. Late Miocene–
814   early Pleistocene paleoclimate history of the Chinese Loess Plateau revealed by remanence
815   unmixing. Geophys. Res. Lett. 41(6), 2163–2168.

816 Peters, C., Austin, W.E.N., Walden, J., Hibbert, F.D., 2010. Magnetic characterisation and
817   correlation of a Younger Dryas tephra in North Atlantic marine sediments. J. Quaternary Sci.
818   25(3), 339-347.

819 Rankey, E.C., Farr, M.R., 1997. Preserved pedogenic mineral magnetic signature, pedogenesis,
820   and paleoclimate change. Pennsylvanian Roca Shale (Virgilian, Asselian), central Kansas,
821   USA. Sediment. Geol. 114, 11–32.

822 Renne, P.R., Deino, A.L., Hilgen, F.J., Kuiper, K.F., Mark, D.F., Mitchell, W.S., Morgan, L.E.,
823   Mundil, R., Smit, J., 2013. Time Scales of Critical Events Around the Cretaceous-Paleogene
824   Boundary. Science. 339, 684-687.

825 Retallack, G. J., Sheldon, N. D., Cogoini, M., Elmore, R. D., 2003. Magnetic susceptibility of
826   early Paleozoic and Precambrian paleosols. Palaeogeogr. Palaeoclimatol. Palaeoecol. 198(3-
827   4), 373-380.

828 Retallack, G.J, 2009. Greenhouse crises of the past 300 million years. Geol. Soc. Am. Bull. 121(9-
829   10), 1441-1455.

830 Retallack, G.J., 1991. Untangling the e!ects of burial alteration and ancient soil formation. Annu.
831   Rev. Earth Planet. Sci. 19, 183-206.

832 Retallack, G.J., 1999. Depth to pedogenic carbonate horizon as a paleoprecipitation indicator?:
833   Comment and Reply. Geology. 27(12), 41-52.

834 Retallack, G.J., 2005. Pedogenic carbonate proxies for amount and seasonality of precipitation in
835   paleosols. Geology. 33(4), 333-336.

836 Russell, D.A., Russell, D.E., Sweet, A.R., 1993. The end of the dinosaurian era in the Nanxiong
837   Basin. Certebrata Palasiatica, 1993, 31(2): 139-145

838 Schulte, P., Alegret, L., Arenillas, I., Arz, J.A., Barton, P.J., Bown, P.R., Bralower, T.J.,
839   Christeson, G.L., Claeys, P., Cockell, C.S., Collins, G.S., Deutsch, A., Goldin, T.J., Goto, K.,
840   Grajales-Nishimura, J.M., Grieve, R.A.F., Gulick, S.P.S., Johnson, K.R., Kiessling, W.,
841   Koeberl, C., Kring, D.A., Macleod, K.G., Matsui, T., Melosh, J., Montanari, A., Morgan, J.V.,
842   Neal, C.R., Norris, R.D., Pierazzo, E., Ravizza, G., Rebolledo-Vieyra, M., Reimold, W.U.,
843   Robin, E., Salge, T., Speijer, R.P., Sweet, A.R., Urrutia-Fucugauchi, J., Vajda, V., Whalen,
844   M.T., Willumsen, P.S., 2010. Response—Cretaceous Extinctions. Science. 328, 975-976.

845 Schwartzmann, D.W., Volk, T., 1991. Biotic enhancement of weathering and surface temperatures
846   of Earth since the origin of life. Palaeogeogr. Palaeoclimatol. Palaeoecol. 90, 357-371.

847 Scotese, C.R., 2014. KT Globe, (KT_Pgeog_357.kmz, Google Earth format),
848   www.globalgeology.com, PALEOMAP Project, Evanston, IL.KT_Pgeog_357

849 Shu, L., Deng, P., Wang, B., Tan, Z., Yu, X., Sun, Y., 2004. Lithology, kinematics and
850   geochronology related to Late Mesozoic basin-mountain evolution in the Nanxiong-
851   Zhuguang area, South China. Sci. China Earth Sci. 47 (8), 673-688.

852 Shunso, I., Hua, R., Mihoko, H., Hiroyasu, M., 2010. REE Abundance and REE Minerals in
853   Granitic Rocks in the Nanling Range, Jiangxi Province, Southern China, and Generation of
854   the REE-rich Weathered Crust Deposits. Resour. Geol. 58(4), 355-372.

855 Sidhu, P.S., 1988. Transformation of trace element-substituted maghemite to hematite, Clay.
856   Miner. 36(1), 31-38.

857 Smith, D.O., 1956. Magnetization of a Magnetite Single Crystal Near the Curie Point. Phys. Rev.
858   102(4), 959-963.

859 Snowball, I., Sandgren, P., Petterson, G., 1999. The mineral magnetic properties of an annually
860   laminated Holocene lake-sediment sequence in northern Sweden. Holocene. 9(3), 353-362.

861 Thompson, R., Oldfield, F., 1986. Environmental Magnetism. London: Allen & Unwin, 1-228.

862 Tong, Y., Li, Q., Wang, Y.Q., 2013. An Introduction to recent advance in the study of the
863   continental Early Paleogene stages in China. Journal of Stratigraphy. 37(4), 428-440. (In
864   Chinese with English abstract)

865 Torrent, J., Barrón, V. Liu, Q.S., 2006. Magnetic enhancement is linked to and precedes hematite

formation in aerobic soils. Geophys. Res. Lett. 33, L02402, doi:10.1029/2005GL024818.

Torrent, J., Liu,Q. S., Bloemendal,J., Barrón, V., 2007. Magnetic enhancement and iron oxides in the upper luochuan loess-paleosol sequence, Chinese Loess Plateau, Soil Sci. Soc. Am. J. 71, 1570–1578

Tramp, K.L., Soreghan, G.S., Elmore, R.D., 2004. Paleoclimatic inferences from paleopedology and magnetism of the Permian Maroon Formation loessite, Colorado, USA. Geol. Soc. Am. Bull. 116, 671.

Van Velzen, A.J., Dekkers, M.J., 1999. Low-temperature oxidation of magnetite in loess-paleosol sequences: a correction of rock magnetic parameters, Stud. Geophys. Geod. 43, 357–375.

Wan, X., Zhao, J., Scott, R.W., Wang, P., Feng, Z., Huang, Q., Xi, D., 2013. Late Cretaceous stratigraphy, Songliao Basin, NE China: SK1 cores. Palaeogeogr. Palaeoclimatol. Palaeoecol. 385(3), 31-43.

Wang, C., Feng, Z., Zhang, L., Huang, Y., Cao, K., Wang, P., Zhao, B., 2013a. Cretaceous paleogeography and paleoclimate and the setting of SKI borehole sites in Songliao Basin, northeast China. Palaeogeogr. Palaeoclimatol. Palaeoecol. 385(5), 17-30.

Wang, C., Scott, R.W., Wan,X., Graham, S.A., Huang, Y., Wang, P., Wu, H., Dean, W.E., Zhang, L., 2013b. Late Cretaceous climate changes recorded in Eastern Asian lacustrine deposits and North American Epieric sea strata. Earth-Sci. Rev. 126, 275-299.

Wang, Y., 2012. Paleoclimate changes of thr Late Cretaceous-Late Paleocene in the Nanxiong Basin, South China. Nanjing University, (in Chinese with English abstract)

Wang, Y., Huang, C., Sun, B., Quan, C., Wu, J., Lin, Z., 2014. Paleo-CO_2 variation trends and the Cretaceous greenhouse climate. Earth-Sci. Rev. 129, 136-147.

Wang, Y., Li, X., Zhou, Y., Liu, L., 2015. Paleoclimate indication of Terrigenous clastic rock's component during the Late Cretaceous-Early Pa;Eocene in the Nanxiong Basin. Acta Sedimentologica Sinica. 33(1), 116-123. (In Chinese with English abstract)

Wilson, P.A., Norris, R.D., Cooper, M.J., 2002. Testing the Cretaceous greenhouse hypothesis using glassy foraminiferal calcite from the core of the Turonian tropics on Demerara Rise. Geology. 30(7), 607-610.

Wu, H., Zhang, S., Jiang, G., Huang, Q., 2009. The floating astronomical time scale for the terrestrial Late Cretaceous Qingshankou Formation from the Songliao Basin of Northeast China and its stratigraphic and paleoclimate implications. Earth Planet. Sc. Lett. 278(3-4), 308-323.

Xie, Q., 2008. Nanominerals of the loess-red clay sequences in Chinese Loess Plateau. Hefei University of Technology. (in Chinese with English abstract)

Xiong, S., Ding, Z., Zhu, Y., Zhou, R., Lu, H., 2010. A ~6 Ma chemical weathering history, the grain size dependence of chemical weathering intensity, and its implications for provenance change of the Chinese loess–red clay deposit. Quaternary Sci. Rev. 29(15), 1911-1922.

Yan, Y., Xia, B., Lin, G., Cui, X., Hu, X., Yan, P., Zhang, F., Geochemistry of the sedimentary rocks from the Nanxiong Basin, South China and implications for provenance, paleoenvironment and paleoclimate at the K/T boundary. Sediment. Geol. 197(1-2), 127-140.

Yang, W., Chen, N., Ni, S., Nan, J., Wu, M., Jiang, J., Ye, J., Feng, X., Ran, Y., 1993. Carbon and Oxygen Isotopic Compositions of the Carbonate Rocks and the Dinosaur Eggshells in the Cretaceous Red Beds and Their Implication for Paleoenvironment. Chinese Sci. Bull. 38(23), 1985-1989.

Ye, J., 2000. Discussion on the problems of the K/T Boundary in the Nanxiong Basin. Certebrata Palasiatica, 38(1), 1-9.

Zachos, J., Pagani, M., Sloan, L., Thomas, E., Billups, K., 2001. Trends, Rhythms, and Aberrations in Global Climate 65 Ma to Present. Science. 292(5517), 686-693.

Zhang X, Li G. Discussion on geological age of the Pingling Member of Shanghu Formation in the Nanxiong Basin,Guangdong Province. Journal of Stratigraphy, 2015,39 (1): 74-80. (In Chinese with English abstract)

Zhang, L., 2016. Paleoclimatic evolution and mechanism of the mass extinction during the K-Pg boundary: Evidences from several terrestrial basins in East China. China University of Geosciences (Beijing). (in Chinese with English abstract)

Zhang, Q., 1981, Paleocene sporopollen assemblages in the Nanxiong Basin Guangdong Province. In: Bull. Yichang Inst. Geol. M. R., Chinese Acad. Geol. Sci. Sp. Iss. S. P. 106-117. (in Chinese with English abstract)

923 Zhang, T., Guo, Z.T., Wu, H.B., Ge, J., Zhou, X., Wu, C., Zeng, F., 2011. Thick Miocene eolian
924   deposits on the Huajialing Mountains: The geomorphic evolution of the western Loess
925   Plateau. Sci. China Earth Sci. 54(2), 241-248.
926 Zhang, W., Erwin, A., Fang, X., Yan, M., Song, C., Cao, L., 2012. Paleoclimatic implications of
927   magnetic susceptibility in Late Pliocene–Quaternary sediments from deep drilling core SG-1
928   in the western Qaidam Basin (NE Tibetan Plateau). J. Geophys. Res. 117(B6), 6101.
929   doi:10.1029/2011JB008949.
930 Zhang, X., 1992. A study on Ostracod fauna of Shanghu Formation and Cretaceous-Tertiary
931   Boundary in Nanxiong Basin, Guangdong. Acta Micropalaeontologica Sinica. 6, 678-702.
932   (In Chinese with English abstract)
933 Zhang, X., Li, S., 2000. New progress in stratigraphic study of the western area of Nanxiong
934   Basin. Guangdong Geology. 15(1), 9-18. (In Chinese with English abstract)
935 Zhang, X., Lin, J., Li, G., Lin, Q., 2006. Non-marine Cretaceous-Paleogene boundary section at
936   Datang, Nanxiong, northern Guangdong. Journal of Stratigraphy. 30(4), 327-340. (In Chinese
937   with English abstract)
938 Zhang, X., Zhang, X., Hou, M., Li, G., Li, H., 2013. Lithostratigraphic subdivision of red beds in
939   Nanxiong Basin, Guangdong, China. Journal of Stratigraphy. 37(4), 441-451. (In Chinese
940   with English abstract)
941 Zhao, G., Han, Y., Liu, X., Chang, L., Lü, B., Chen, Q., Guo, X., Yan, J., Yan, J., 2016. Can the
942   magnetic susceptibility record of Chinese Red Clay sequence be used for palaeomonsoon
943   reconstructions?. Geophys. J. Int. 204(3), 1421-1429.
944 Zhao, Z., Mao, X., Chai, Z., Yang, G., Zhang, F., Yan, Z., 2009. Geochemical environmental
945   changes and dinosaur extinction during the Cretaceous-Paleogene (K/T) transition in the
946   Nanxiong Basin, South China: Evidence from dinosaur eggshells. Chinese Sci. Bull. 54(5),
947   806-815.
948 Zhao, Z., Yan, Z., 2000. Stable isotopic studies of dinosaur eggshells from the Nanxiong Basin,
949   South China. Sci. China Earth Sci. 43(1), 84-92.
950 Zhao, Z.K, Mao, X.Y., Chai, Z.F., Yang, G., Kong, P., Ebihara, M., Zhao, Z., 2002. A possible
951   causal relationship between extinction of dinosaurs and K/T iridium enrichment in the
952   Nanxiong Basin, South China: evidence from dinosaur eggshells. Palaeogeogr.
953   Palaeoclimatol. Palaeoecol. 178(1-2), 1-17.
954 Zhao, Z.K., Ye, J., Li, H.M., 1991. Extinction of the dinosaurs across the Cretaceous-Tertiary
955   boundary in Nanxiong Basin, Guangdong Province. Certebrata Palasiatica. 29(1), 1-20. (in
956   Chinese with English abstract)
957 Zhou, L.P., Oldfield, F., Wintle, A.G., Robinson, S.G. Wang, J., 1990. Partly pedogenic origin of
958   magnetic variations in Chinese loess. Nature. 346, 737–739.
959